

Outburst floods of the Maly Yenisei. Part II – new age constraints from Darhad basin

Jigjidsurengiin Batbaatar  and Alan R. Gillespie

Quaternary Research Center, University of Washington, Seattle, WA, USA

ABSTRACT

Some of the largest cataclysmic floods of the Quaternary followed multiple breaches of glaciers damming the headwaters of the Maly Yenisei river in southern Siberia. The shorelines of the impounded lake in Darhad basin suggest at least four depths of 290, 175, 145, and 65 m. Fossil evidence, together with previous ^{14}C and luminescence dating, indicates the existence of a deep lake during MIS 3; the eroded character of the highest shoreline suggests that the deepest lake was older. ^{10}Be dating of moraines in the surrounding mountains has documented major glacial advances during MIS 2, although no published direct dating has confirmed a highstand of the lake then. To address this problem, we extracted lake sediments from a 92.6 m deep borehole, sampled beach sands from the nearby basin edge, and dated them both using luminescence methods. We also dated, with ^{10}Be , the eroded remnants of the end moraine deposited by the last glacier that dammed Darhad basin, as well as other moraines in the mountains surrounding the basin. These numerical ages confirm that a deep lake existed in Darhad basin at ~ 20 ka and that a large glacier crossed the Maly Yenisei and dammed Darhad basin at ~ 21 ka. The deep lake persisted episodically until ~ 14 ka. The ^{10}Be dating in the surrounding mountains shows that the MIS 2 glaciers subsequently retreated but stalled or re-advanced at ~ 12 , 10, and 1.5 ka. ^{10}Be dating from the central massif of Mongolia is consistent with this chronology and confirms that MIS 3 equilibrium-line altitudes were slightly (~ 75 m) lower or approximately the same as those of the MIS 2. The temporal and spatial patterns of glacial advances in southern Siberia and central Mongolia coincided with those of glacial advances in similar climate conditions of the Altai mountains.

ARTICLE HISTORY

Received 28 March 2016

Accepted 20 May 2016

KEYWORDS

Outburst floods; megafloods; cataclysmic floods; glacial dams; Maly Yenisei; Bolshoy Yenisei; palaeolake Darhad; Darhad basin; Sayan

1. Introduction

The cataclysmic floods down the Yenisei river in Siberia (Figure 1) were among the largest on Earth according to their estimated discharge rates (O'Connor and Costa 2004). The high abandoned terraces and giant gravel dunes in the Kyzyl basin (Figure 1; Batbaatar and Gillespie 2015) provide evidence for the large floods of the Yenisei. However, no flood deposits have yet been directly dated. The largest of the floods on the Maly Yenisei came from Darhad basin in northern Mongolia, which during the Pleistocene held lakes up to 290 m deep and with a volume of up to 809 km^3 (Komatsu *et al.* 2009). At the end of the Pleistocene Epoch, the lakes were impounded by glaciers, especially the Tengis glacier, an outlet glacier from the East Sayan ice field (Figure 2) (Merle 2001; Krivonogov *et al.* 2005; Gillespie *et al.* 2008). At its maximum extent, the Tengis glacier created a series of high ice dams. The outwash gravels

from the retreating Tengis glacier subsequently created lower gravel dams at the same location (Krivonogov *et al.* 2005; Batbaatar and Gillespie 2015).

The ages of the heretofore undated dams are controversial. Krivonogov *et al.* (2005) proposed that the Tengis glacier grew large enough to dam Darhad basin during or before Marine Oxygen Isotope Stage (MIS) 3.¹ They based this deduction on (1) two observations from Darhad basin itself, and (2) two telecorrelations. In regard to (1), Gravis and Lisun (1974) reported a high abundance of tree pollen in lake sediments in Darhad basin, which suggested to them a warmer climate of the MIS 3 Karginian Interstadial, and Krivonogov *et al.* (2005) reported wood remains in deltaic sediments near Talyn lake, on the floor of the basin, that yielded three ages near the limit of the ^{14}C method, $>46,080$, $>46,090$, and $\geq 44,900 \pm 1200$ ^{14}C year. In regard to (2), telecorrelations with moraines of the local Last Glacial Maximum (LGM_L; e.g. Gillespie and Molnar 1995) ~ 130 km NE of

CONTACT Jigjidsurengiin Batbaatar  bataa@uw.edu  Quaternary Research Center, University of Washington, Seattle, WA, USA
 Supplemental data for this article can be accessed [here](#).

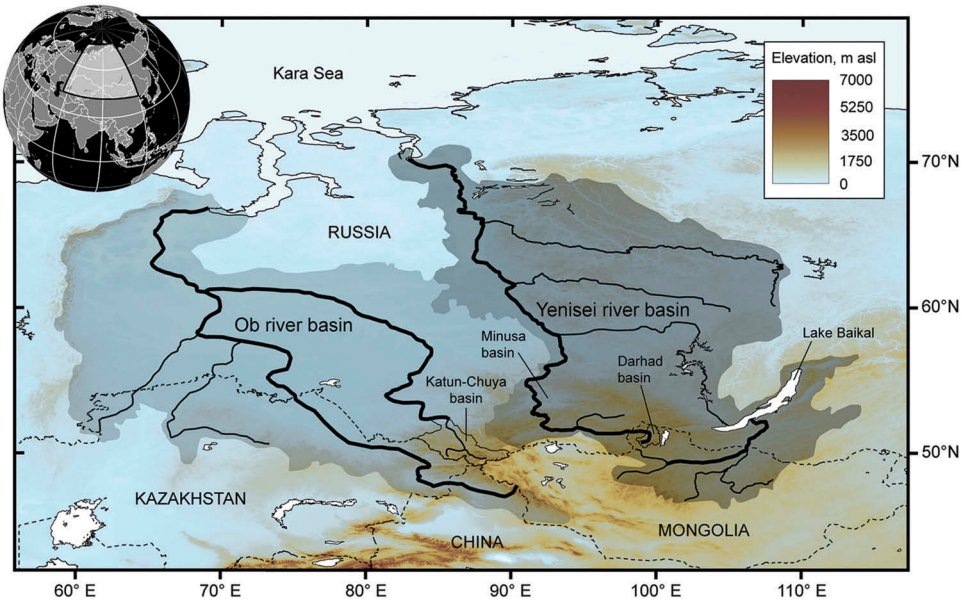


Figure 1. The largest Pleistocene floods in Siberia originated from the Katun–Chuya river basin (headwaters of the Ob river) and from Darhad basin (headwaters of the Yenisei river). Background: Shaded-relief image produced from 90 m SRTM elevation data (Farr *et al.* 2007). Colour version is available online.

Darhad basin (Figure 1) that have two thermoluminescence ages of ~70 ka (Shchetnikov 2001), may indicate that the LGM_L in Darhad basin was similarly early, such that the glacial lakes there most likely predate MIS 3. Krivonogov *et al.* (2005) reasoned that because the favourable conditions for a development of Siberian glaciation occurred during the MIS 5d interstadial, as inferred from the glacial sediments identified in the Lake Baikal cores (e.g. Prokopenko *et al.* 2001), large MIS 2 glaciers in Darhad were unlikely.

In short, Krivonogov *et al.* (2005) contended that no large lakes existed in Darhad basin after MIS 3, that only the Tengis sediment dams could have impounded lakes during MIS 2, and that those lakes must therefore have been shallow. But Krivonogov *et al.* (2005) offered no direct evidence of the timing of the deepest lakes.

Gillespie *et al.* (2008) dated glacial deposits using cosmic-ray exposure (CRE) (¹⁰Be) analysis and dated the lake sediments using radiocarbon and luminescence analysis in and around Darhad basin. They found that the glaciers around the basin advanced to their maxima during MIS 3, and that the MIS 2 glaciers were likely slightly smaller but big enough to impound at least the 145 m deep lake. These findings appeared to rule out the two telecorrelation arguments of Krivonogov *et al.* (2005), but not those from the observations in Darhad basin. Indeed, Gillespie *et al.* (2008) confirmed with ¹⁴C and luminescence dating the conclusions of Gravis and Lisun (1974) that the lake sediments at the Shargyn river cutbank (Figure 2) were from MIS 3. Gravis and Lisun

(1974) also reported younger lake sediments in this area with a high content of moss pollen that they assigned to the cold climate of MIS 2 Sartan Stade. However, Gillespie *et al.* (2008) could not find MIS 2 sediments in the cutbank of the Shargyn river, and they suspected that Shargyn vicinity was prone to erosion during the sudden draining of the palaeolakes, and that possibly any MIS-2 lake sediments were eroded then. Lastly, Krivonogov *et al.* (2005) evidently did not consider the possibility that the ≥45 ka wood from the Talyn delta could have been reworked from older deposits.

The above outlines the current state of the ‘controversy’ concerning the timing of the last deep palaeolake. In this article, we present new chronological data for the long drill cores we extracted from the Darhad basin, intended to determine the timing of the most recent Pleistocene lakes there. These data by themselves cannot establish the depth of those lakes, so we also dated associated shoreline deposits with measured elevations. The lake sediments do not directly link the palaeolake to the hypothesized but eroded glacier dam. The end moraine left by the Tengis outlet glacier (Figure 2) – evidence that the glacier indeed crossed the Maly Yenisei to impound a large lake behind it – has not been definitely dated until now. If ¹⁰Be ages for the end moraine show that the latest dams indeed occurred during MIS 2, the existence of the palaeolake then and its depth, plus the linkage to the glacier dam, would all be established and the controversy would be resolved.

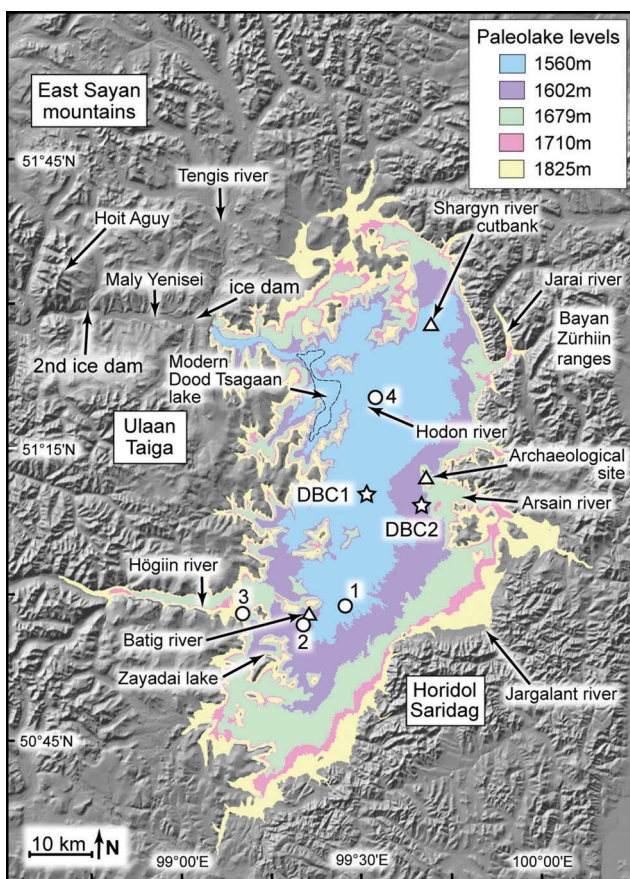


Figure 2. Darhad basin map (with lake levels): Geographic names and the extent of the palaeolake when Darhad basin filled to 1560, 1602, 1679, 1710, and 1825 m asl (successive shades of grey; colour version is available online). Circles numbered 1, 2, 3 indicate wells of Ufland *et al.* (1971), and 4 indicates the DDB10-3 core (Krivonogov *et al.* 2012). Star symbols indicate two cores presented in this article. Triangles are ^{14}C -sampling sites. Shaded-relief image from SRTM data. The map is from Gillespie *et al.* (2008).

2. Methods

In this section we describe the methods used for drilling the boreholes in Darhad basin, the physical investigation and analysis of the sediments, and the methods for dating the sediments from the core as well as from the beach and moraines. We also describe the methods we used to estimate the equilibrium-line altitudes (ELAs) in order to provide a regional spatial pattern against which to validate the local dated palaeoglacier sequences. We provided a Google Earth kmz file (online supplementary material) that marks all the geographic features discussed in Part I (Batbaatar and Gillespie 2015) and in this article, as well as the locations of the new dating sites we present in this article.

2.1. Drilling and sediment-extraction methods

In November 2004, three boreholes, DBC1A and B at 1547 m asl, and DBC2 at 1583 m asl, were drilled in Darhad basin to study the sediments of palaeolake Darhad and to date them with luminescence methods. DBC1A was 92.6 m long, but from depths of 2–4 m segregation ice was encountered and the core was not recovered intact. Longer sections of lake sediments proved to be difficult to extract from the steel tubes, and below 4 m the core was recovered in short ~40–80 cm segments. Therefore, a second borehole, DBC1B (10.6 m deep), was drilled ~20 m from DBC1A specifically to sample the uppermost lake sediments and complete the top of core DBC1A. The stratigraphies for cores DBC1A and B are combined and treated as though taken from a single core, 'DBC1', as shown in Figure 2.

Another shallow core, DBC2 (14.1 m), was located closer to the eastern edge of the palaeolake (Figure 2). It was drilled through a gravel dune field, likely of outwash, from either the Arsain or Jargalant river. The core was extracted to find and examine the base of the outwash and to look for datable material, but none was found and the core was not described fully.

In the field, we visually inspected the cores DBC1A and DBC1B, measured magnetic susceptibility, and examined the lithology of sediments to determine the suitability of sands for luminescence dating. The cores were then split into halves for photography and subsampling of sediments and organic materials. Half of each core was stored in boxes and later sent to the Institute of Geology and Mineral Resources (Mongolian Academy of Sciences) in Ulaanbaatar for storage. Sergey Krivonogov (Institute of Geology and Mineralogy, Siberian Branch of the Russian Academy of Sciences) took detailed photos of the archived core in 2007. The archived core was later cut into small pieces and moved to the Siberian Branch of the Russian Academy of Sciences, Irkutsk, for grain-size analysis and magnetic inclination measurements. Labelled pieces of DBC1 in ~5 or 10 cm increments are now stored at the University of Washington and the Mongolian Academy of Sciences.

2.1.1. Grain-size analysis

Grain sizes of the sediments in the DBC1 were measured at the Institute of Petroleum Geology of the Siberian Branch of RAS, using the equipment Microtrac X100 and Microtrac ASVR. The samples were prepared from the core at intervals of 5 or 10 cm.

2.1.2. Magnetic susceptibility

Sediment influx to a basin increases due to greater erosion during the glacial advances, which tend to correlate with higher concentrations of magnetic minerals in high-latitude and high-altitude environments (Verosub and Roberts 1995). To document the temporal variation in the sediment influx to Darhad basin, we measured the magnetic susceptibility in the field as cores DBC1A and B were extracted, but for only the top 35 m. The Bartington MS2 metre with a MS2E sensor then froze and could not be operated in ambient temperatures that ranged down to -30°C . We measured the magnetic susceptibility on the archived core later in Ulaanbaatar. Repeat measurements on the top segment of the core agreed with the existing field measurements.

2.1.3. Borehole temperature

We used a conventional mercury thermometer to measure the temperatures in the borehole DBC1A. The thermometer was lowered and left in the well at a particular depth for ~ 10 min to equilibrate with the borehole temperature. The uncertainty of the thermometer is $<0.5^{\circ}\text{C}$.

2.1.4. Diatom counting

We subsampled the archive core in 2013 to examine the diatom assemblages in the DBC1 core at the depth of 78.9–79.8 m. The subsamples were 2 cm long, taken at every 10 cm depth interval of the 1 m segment. Brian L. Sherrod (US Geological Survey) prepared the samples and performed the species identification and counting of the diatom fossils. The sediments were disaggregated in HCl and then treated with 30% H_2O_2 . The resulting diatom-rich material was dripped onto a cover slip and allowed to evaporate over gentle heat. Then the slides were prepared using the Cargille Meltmount™ media and the counts consisted of ~ 200 valves of diatoms per slide. General environment of the diatom species is taken from AlgaeBase (Guiry and Guiry 2015).

2.2. Dating

For this study we dated sediments with luminescence and ^{14}C techniques, and boulders from moraines by their cosmic-ray exposure (^{10}Be ; Figure 3).

2.2.1. Luminescence dating

We used several dating methods as required by the nature of the samples collected. These included both optically stimulated luminescence (OSL) and infrared-stimulated luminescence (IRSL) techniques and the single-aliquot regenerative (SAR), the double SAR, and the pulsed-measurement methods.

2.2.1.1. Sites and sampling procedures. For luminescence dating, we sampled lake sediments from the DBC1 core, beach sands on the range front near the Arsain river, and the terminal moraine in the Sarig valley. If the core segment appeared to contain datable sand, it was not split until night, so that it could be sampled in the dark. The samples were wrapped in aluminium foil, and placed in light-proof bags for shipment to the laboratory at the University of Washington. When this approach was not feasible, samples were wrapped in aluminium foil immediately upon extraction (exposure: ~ 5 s) and transported to the laboratory in light-tight containers. The exposed exterior was shaved off in the dark laboratory and saved for radioactivity measurements. The inner core was re-packaged into lightproof plastic tubes. The sediments to be dated were extracted from the unexposed interior of the archived core.

Sample DB-AG-2007-02, from the end moraine of the Tengis glacier, was extracted using hand-augers and was wrapped in aluminium foil immediately after extraction. The inner parts were subsampled later in the darkroom. The beach sands near the Arsain river, sample DB-AG-2004-03A, were sampled directly by driving light-proof tubes into the deposit. Later in the dark laboratory, the exposed sediments at both ends of the tube were removed for radioactivity measurements, and only the inner parts of the sample were used for luminescence measurements.

2.2.1.2. Analysis of the luminescence data. The sediments were prepared and analysed in the Luminescence Laboratory, University of Washington, under the guidance of James Feathers. Luminescence measurements were made on both quartz and feldspar. Coarse (150–212 μm) and fine (1–8 μm) grains of quartz and feldspars were separated from each of the bulk samples following the chemical procedures of Feathers *et al.* (2012). We measured the luminescence in the coarse grains following the single-aliquot regenerative (SAR) protocol (Wintle and Murray 2006) modified for feldspars (Auclair *et al.* 2003). Multi-mineral aliquots of fine grains were analysed using the double SAR method (Banerjee *et al.* 2001) and pulsed measurements (Feathers *et al.* 2012). Feldspar measurements were corrected after the fading assessments (Huntley and Lamothe 2001; Auclair *et al.* 2003). We estimated several equivalent dose (D_{e}) values for the same sample using minimum and central values from the age histogram (Galbraith and Roberts 2012), and also finite mixture modelling (Galbraith and Green 1990; Jacobs *et al.* 2006). Detailed explanations of the luminescence dating methods are given in the online supplementary material.

2.2.2. ^{14}C dating

We used ^{14}C analysis opportunistically to date samples of charcoal, wood, and peat from lacustrine and paludal sediments of Darhad basin and paludal and fluvial sediments related to the outlet glaciers of the East Sayan ice field in Siberia. The thin peaty layers in the lacustrine sediments developed during lake regressions.

2.2.2.1. East Sayan, the profile samples. Paludal sediments accumulated against a left-lateral moraine of the outlet glaciers in the Sentsa river valley after the LGM_L, ~6 km upriver from the terminal position of the glacier (Vasil'chuk *et al.* 2015). A ~2.5 m section is exposed in the bank of a thermokarst lake, and this was sampled for ^{14}C analysis. The uppermost 12 cm consists of loess. From 12 to 20 cm is a charcoal-bearing buried A horizon. Below is fine sand, and a lens of segregation ice at 200 cm. One charcoal sample was taken from the buried horizon and four samples of reeds and grass were taken from depths of 60, 73, 172, and 195 cm. The sediments were dated to help establish the post-glacial evolution of the valley as well as to possibly obtain a limiting minimum age for the Sentsa glacier.

Against a right-lateral moraine of the Oka river valley is a sand quarry whose base is in fluvial cobbles ~10 m above river level. Above the likely outwash are ~4.5 m of cross-bedded sand. The sands may be from an ice marginal lake, in which case the outcrop provides the opportunity for a close minimum limiting age for the Oka glacier. We collected two samples of wood fragments from 315 and 432 cm depth to test this possibility.

2.2.2.2 Darhad basin sediments. We collected two near-surface (depth ~10 cm) samples, of peat and woody roots, from near the Batig river, on the western edge of the depocentre of the basin and in an area of active thermokarst. We collected these samples to see if the topmost sediments here and at Shargyn river cutbank (Gillespie *et al.* 2008; Batbaatar and Gillespie 2015) have the same age.

We also collected a sample of charred larch wood from a palaeosol in sand dunes NE of the Arsain river, near the eastern edge of Darhad basin. The site was on the rim of a half-circular ridge that Gillespie *et al.* (2008) proposed to be a possible end moraine that formed underwater, although no glacial deposits have been identified in the valley upstream (this is also the case for the clearly glaciated Jarai valley). There are large (~10 m high) mounds in this hummocky terrain, which Ishikawa and Yamkhin (2015) interpreted as permafrost pingos. It is possible that the pingos were formed inside the wide (~1.5 km) end moraine (?) of the Arsain glacier,

just as permafrost features occur behind the end moraines at the nearby Jarai river. We dated the charcoal at Arsain river to establish a confident minimum age for the putative Arsain moraine.

Lastly, we collected two more samples from the Shargyn river cutbank. They were peat from ~8 m depth, and were taken from unconformities near the southern end of the cutbank where the stratigraphy has been affected by slumping, but where nearby sediments dated by Gillespie *et al.* (2008) suggested an age near the ^{14}C limit of 45 ka. This is an important outcrop for understanding the chronology of the Darhad palaeolake, and we collected these samples to confirm the MIS 3 ages of this southern section.

2.2.2.3 ^{14}C sample treatment and data analysis. In the field, the collected samples were brushed to remove adhered sand and silt, placed in small plastic bags or photographic film canisters, and air-dried as soon as feasible. They were transported to the laboratory at UW in dark containers. In the lab, coarse samples were cleaned again with a brush. Coarse stems were hand selected from peat samples and grass samples. About 0.5 g of each sample was transferred to glass vials for mailing to a laboratory for measurement. ^{14}C was measured at the Center for Acceleration Mass Spectrometry (CAMS) of the Lawrence Livermore National Laboratory in California. No correction for hard-water effects was necessary because no shells were dated, only land plants.

2.2.3. Cosmic-ray exposure dating (^{10}Be)

CRE analysis was used to date till boulders exposed on moraine crests. The number of suitable boulders on our key site, the end moraine of the Tengis glacier, was limited. We also dated other moraines from the region in order to establish a regional chronology of late Quaternary glaciation near Darhad basin.

2.2.3.1 Sampling sites. We collected CRE samples from three general areas: Darhad basin and along the Maly Yenisei; the East Sayan mountains; and the central massif of Mongolia. Samples from the first group were intended to determine when glaciers dammed the Maly Yenisei; the second group was to improve the glacial chronology for the Darhad region; and the third group was intended to test how reliably glacial chronologies could be extended geographically – i.e. did East Sayan ages also apply to the Darhad basin ~150 km to the south? Sample sites are shown in Figure 3.

2.2.3.2 Group 1. Group 1 contained sites at the mouth of the Tengis river, the Hoit Aguy massif, and the

headwaters of the Jarai river. We sampled the undated terminal moraines of the late Pleistocene Tengis glacier, thought to have crossed the Maly Yenisei and dammed the Darhad palaeolakes. Its termimoraines blocked the mouth of the north-flowing Sarig river, south of the Maly Yenisei. Therefore, dating the Tengis terminals directly dates the impounding of the palaeolakes and, approximately, at least one of the catastrophic outburst floods.

We also mapped and sampled moraines of the eastern side of the Hoit Aguy massif, a high ridge near the Tuvan–Mongolian border that rose above the south-flowing outlet glaciers of the East Sayan ice field. One goal in doing so was to date another possible glacier dam across the Maly Yenisei ('2nd ice dam' in Figure 2; Komatsu *et al.* 2009); another goal was to establish a dated palaeo ELA.

The final site from Group 1 was in the headwaters of the Jarai river, for which LGM_G piedmont moraines were dated by Gillespie *et al.* (2008). The site was on a pass that separated the Jarai drainage from a local ice cap to the north that at its maximum extent fed ice south across the pass and into Darhad basin. During deglaciation, the sampled granitic boulders were left on the pass as erratics; their only possible source was north of the pass. Dating these erratics intended to provide an age for the end of the LGM_L in the Darhad area, and thus a minimum age for the ice-dammed palaeolakes and the catastrophic outburst floods from them.

2.2.3.3 Group 2. We also sampled in 2002, with Sergei Arzhannikov, Anastasia Arzhannikova, Vladimir Sheinkman (all: Russian Academy of Sciences, Siberian Branch), and Paul Gillespie, and dated boulders from different moraines on the northern margin of the East Sayan ice field. Arzhannikov *et al.* (2012) later resampled and dated (¹⁰Be) boulders from Pleistocene moraines from the same area. Our new ages, from the original sampling, augment this chronology and add to its scope significantly by including late Pleistocene retreat moraines and Holocene moraines from the only remaining glaciated peak in the East Sayan, Mönh Saridag, north of Hövsgöl lake.

2.2.3.4 Group 3. To test the heterogeneity of late Pleistocene glacier variations in the vicinity of Darhad basin, we also sampled (in 2000) and dated (¹⁰Be) boulders from moraines near Gyalgar peak, the closest (~340 km) massif to the south that was glaciated during the Pleistocene. These new ages augment the dating efforts by Rother *et al.* (2014) at Otgontenger peak, ~130 km further southwest in the Hangai mountains.

2.2.3.5 Sampling protocol. Where possible we sampled large granitic boulders (>1 m in diameter) sitting within 2 m of moraine crests to minimize post-depositional disturbances of boulders. In contrast, Hallet and Putkonen (1994) and Putkonen and Swanson (2003) recommended that the preferred location for sampling was the intersection point between erosion (crest) and aggradation (toe slope) because boulders there were neither exposed by erosion nor shielded by burial, but in permafrost regions such as northern Mongolia solifluction removes material from the flanks of moraines, eliminating this advantage. The boulders were selected to meet the criteria of having minimal erosion: a 'fresh' appearance with few surface irregularities (pits, pans), and no apparent burial or exhumation history. Surfaces with indications of erosion, such as spalling, eroded fractures, or rainwater pits, were not sampled. We collected the rock samples by chisel from the top of the boulders, at least 50 cm above the ground, to minimize burial history. The locations of the samples were recorded in the field using hand-held GPS, or 1:50000 topographic maps. Topographic shielding from the horizon was measured by clinometer.

2.2.3.6 Analysis. We sent the rock samples to the chemical laboratories at the University of Washington and the Hebrew University of Jerusalem, where the quartz was separated by the chemical processing methods of Stone (2000) following Ditchburn and Whitehead (1994). ¹⁰Be/⁹Be ratios were measured at the Lawrence Livermore National Laboratory, and at the Australian Nuclear Science and Technology Organisation. The data were converted to ¹⁰Be concentrations using the sample weights, following Balco (2006). The sample locations, elevation, and other ¹⁰Be data are summarized in Appendix Table A1.

¹⁰Be ages were calculated using CRONUS-Earth version 2.2 (Balco *et al.* 2008). We used the globally calibrated ¹⁰Be production rate of Heyman (2014), which is $3.99 \pm 0.22 \text{ atoms g}^{-1} \text{ year}^{-1}$ when referenced to the scaling of Stone (2000). All calculations of ¹⁰Be ages assumed zero erosion and burial, and we did not account for neutron shielding by snow. The sensitivity analysis of the CRE age estimations to erosion, scaling scheme, and snow cover is given in detail in the online supplementary material: Figure S1; Tables S1 and S2.

2.3. Equilibrium-line altitude (ELA) estimation

Glacier growth responds primarily to precipitation as snow and summer temperatures, with ice accumulating at higher elevations and then flowing downhill. ELAs are the altitude at which balance between accumulation

and ablation is achieved. Where modern glaciers are found and the current ELAs can be determined, the relative lowering of ELA in the past glaciations (Δ ELA) is routinely used as a climate proxy. If the climatic drivers of glacier growth are constant or vary smoothly, ELAs offer a method of telecorrelation for palaeoglaciers. This is helpful in validating CRE ages estimated from small number of samples. In this study, we use ELAs as such a ‘reasonableness’ test for CRE ages for moraines, comparing Darhad ages with those of nearby palaeoglaciers with similar ELAs. Some ELAs have already been published, and we added to this database our own new data for this study (see details in online supplementary material).

2.3.1. Alpine palaeoglaciers

Palaeo ELAs must be determined from the distribution of glacial deposits, since the ancient glaciers no longer exist. The techniques of ELA estimation mentioned below are applicable on modern glaciers as well as on these deposits. Where possible, we used GPS measurements of elevation; elsewhere we used elevations from Google Earth. Our favoured method was the MELM (maximum elevation of the lateral moraine) approach, which equates the ELA with the elevation of the highest lateral moraine (Andrews 1975; Meierding 1982; Porter 2001). The MELM approach is valid only if the lateral moraine has not been covered by talus or eroded. If that was the case we estimated the ELA from the toe-to-headwall ratio (THAR: Charlesworth 1957; Manley 1959), using the threshold value of 0.58 determined for the Darhad region by Gillespie *et al.* (2008). We also estimated ELAs by comparing the areas of accumulation and ablation from the surface topography of palaeoglaciers as reconstructed from ASTER (Advanced Spaceborne Thermal Emission and Reflection Radiometer) digital elevation models (GDEM version 2) (National Aeronautics and Space Administration 2015). Then the ratio of accumulation area to the total area of the palaeoglacier (AAR: Meier and Post 1962; Porter 1975; Gross *et al.* 1976; Torsnes *et al.* 1993) was calculated to find the palaeo ELAs, using a threshold value of 0.6 ± 0.05 determined locally by comparison to MELM ELAs. According to Meierding’s (1982) comparison of different methods for the Front Range in Colorado (USA), the most reliable ELA estimations for the front ranges of Colorado were by the THAR and AAR methods, whereas the MELM was less reliable. On the other hand, in a different setting in the Sierra Nevada of California (USA) Gillespie (1991) and in the tropical Andes (central Peru) Ramage *et al.* (2005) considered the MELM technique to be the simplest and most reliable. Comparisons with ELAs calculated by the THAR

and AAR methods there indicated agreement within ~100 m.

2.3.2. Ice caps and outlet palaeoglaciers

Estimating the ELA for ice caps and outlet glaciers from ice fields is more complicated and less reliable than for alpine valley glaciers. For modern ice caps the ELA lies between the crest and the perimeter, but for palaeo ice caps the highest elevation is unknown so the THAR approach is difficult to use. In addition, the accumulation area usually covers multiple cirques and high plateaus, and the ice-flow patterns are hard to estimate from the bedrock topography alone. Drainage basins within the palaeo ice cap are accordingly hard to define (AAR; cf. Torsnes *et al.* 1993). The MELM approach applied to moraines of outlet glaciers may provide at least a lower limit to the ELA. Therefore, we used the MELM and THAR approaches, using the highest point in the bedrock topography within the estimated watershed of the outlet glacier for the headwall altitude.

3. Results

In this section, we first present the physical characteristics of the lake sediments in DBC1 core. Then we present age constraints for the Darhad palaeolakes from luminescence and ^{14}C dating of lake sediments, and from ^{10}Be dating of the Tengis end moraine. Finally, we provide new results on chronology and extent of the palaeoglaciers in the vicinity of Darhad basin.

3.1. Physical characteristics of lake sediments in DBC1 core

3.1.1. Grain-size analysis

The stratigraphy of the sediments in the DBC1 core is summarized in Figure 4. The upper 1.5 m of the DBC1 core consists of reworked sandy lacustrine silt. It is equivalent to the surface layer at the Shargyn river cutbank described by Gillespie *et al.* (2008), which was ^{14}C dated to ~3.5 cal ka BP. This upper section was lighter-toned than the lower section, probably because carbonates have coated the fine sands. Below 1.5 m the core is dominated by darker-coloured clayey lacustrine silt, rhythmically bedded at a scale of ~1 mm. Sparse shells of pelecypods (*Sphaerium simile?*) and gastropods (*Lioplax subcarinata*, and *Gyraulus deflectus?*) were scattered throughout this lower section. The upper section of 0–11 m is generally sandier than the lower part of the core, with thin layers of (~10 cm) fine sands at depths of ~9 and ~10 m. Other thin sandy layers were encountered at 13.4 and 16.10 m. From 16.1 to 39 m, the core is clayey to sandy silt, coarsening below ~31 m depth. A

series of fine sandy layers occur between 39 and 49.5 m, with the thickest layer occurring at 41.2–44.0 m depth. Well-preserved gastropod and disarticulated bivalve shells were found occasionally. From 49.5 to 70 m the sediments are approximately uniform clayey silt, layered at scales of 1 mm to 1 cm. Below 70 m, to the bottom of the core, are scattered sandy silt layers. The most prominent of these sandy layers were at 77.0–77.5 m depth. From 79 to 80 m there is a distinctive carbonate layer, unique in that it is largely free of clastic material. This layer is fissile, and contains abundant plant remnants, amorphous cyanobacterial and algal material, freshwater sponge spicules, sparse freshwater diatoms, and numerous opaline phytoliths (from grass). There are also shells of shallow water gastropod limpets (*Ferrisia* sp.). These air-breathing limpets feed on diatoms and other algae scraped from the surface, and are highly tolerant of desiccated environments, suggesting a largely dry lake. Below the carbonate layer, to the bottom of the core at 92.6 m depth the sediments are again dominated by clayey silt.

In contrast to the cores of Ufland *et al.* (1969), extracted from nearer to the basin depocentre, fewer lenses of segregation ice were encountered in DBC1. The length of drilling tubes dictated the lengths of the core segments, and sedimentary structures such as ice lenses or the stratigraphic boundaries were recovered intact within the segments.

3.1.2. Magnetic susceptibility

The volume magnetic susceptibility values for the core DBC1 are shown in Figure 4. The magnetic susceptibility values were higher and varied significantly in the upper 60 m of the core, averaging at 47.7 ± 30.6 ($10^{-6} \text{ cm}^3 \text{ g}^{-1}$ CGS $\pm 1\sigma$). We interpret the high values as corresponding to increased erosion in the mountains around Darhad basin, probably due to glacial advances. High concentrations of magnetic minerals in the Lake Baikal sediments were also correlated with glacial intervals (Peck *et al.* 1994). In contrast, the sediments at lower depths of 60–92 m exhibit low magnetic susceptibility, averaging 13.6 ± 5.8 ($10^{-6} \text{ cm}^3 \text{ g}^{-1}$ CGS $\pm 1\sigma$), indicating that the influx of magnetic minerals to the basin were low and did not vary much during this time. In addition, the fewer number of sedimentation breaks below 60 m implies a stable glacier and continuous dam during this period.

In general, coarser grain size due to rapid erosion and high runoff correlates well with an increase in the magnetic susceptibility (Verosub and Roberts 1995). However, the 0.65 m thick massive fine sand layer at the depth of 76.9 m had a very low magnetic susceptibility similar to silts above and below this layer,

suggesting that the increased grain size there is not related to increased runoff. Above these massive sands, a thin layer of cross-bedded sands is sandwiched between silt layers at 76.7 m (Figure 4; Table A2), suggesting a rapidly fluctuating lake. This layer is very close to the massive sands at 76.9 m, which could have been locally reworked in the palaeolake, probably due to wave action of a shallow lake or slumping in a deep lake.

3.1.3. Temperatures in the borehole

The temperature in the well averaged around -1°C , but ranged between $+1^\circ\text{C}$ near the surface and -2.7°C at ~ 6 m depth (Figure 4). The depth of the modern active layer near Shargyn river is ~ 3 m (Sharkhuu *et al.* 2007). The ice content in the sediments decreased below 40 m depth in the core DBC1. Between the depths of ~ 6 and 12 m the temperature decreased rapidly to -1°C , then it increased gradually until the bottom of the borehole when it was -0.7°C . The thermal gradient in the lower portion of the borehole is much lower than the geothermal gradient for crust (global average $25\text{--}30^\circ\text{C km}^{-1}$; Fridleifsson *et al.* 2008), which could be explained by low thermal conductivity of ice-poor lake sediments (Clauser and Huenges 1995; Cortes *et al.* 2009; references therein) that cover Darhad basin to a depth of at least 200 m (Ufland *et al.* 1971).

3.1.4. Sedimentation breaks in the DBC1 core

Most of the silt-dominated sections show horizontal laminations of sediments having repeated alternation in colour and composition (rhythmites). The changes in sediment are likely seasonal and the sediments are likely varves, but in absence of a densely dated section this is hard to establish with certainty, especially for a lake with episodically fluctuating depth. However, these rhythmic sediments were disturbed, or partially removed many times due to different processes, showing that the sediment record in the DBC1 core is not continuous (Batbaatar *et al.* 2012). Although many of the breaks are disconformities of uncertain depositional significance, we identified 25 unconformities in the DBC1 core, including disturbance due to turbidity currents, cross-beds, deformed layers, erosion surfaces, and a micro-fault. These are summarized in Appendix Table A2. We note that the number of identified unconformities is likely a minimum; probably there are more disturbances throughout the core.

The discontinuous records of lake sediments in the DBC1 core are consistent with the idea of Grosswald and Rudoy (1996) that the palaeolakes in Darhad basin repeatedly drained and filled. They also show that a linearly interpolated deposition age between any two

independently dated sections is unreliable, unless continuous deposition between them can be demonstrated. Therefore, a dating method that relies on the assumption of a constant sedimentation rate, such as correlation of magnetic inclinations (e.g. Krivonogov *et al.* 2012), should only be used with care on the records from the DBC1 core. Furthermore, as other sections such as the cutbank of the Shargyn river (e.g. Gillespie *et al.* 2008) likewise contain angular unconformities suggesting episodes of coarse-scale slumping or erosion, and as such features may be widespread in the basin, age models for any sections or cores from Darhad basin must be used cautiously.

3.1.5. Diatom assemblages at 79–80 m depth

The 1 m layer below 79 m depth was distinct from the other lake sediments in the DBC1 due its clast-free and carbonate-rich composition. Within it, the diatom assemblages were largely restricted to two or three species, especially in the lower 50 cm of the layer. The low diversity of diatoms suggests that at this time the Darhad palaeolake existed under stable conditions. However, the number of fossils varied considerably over the section, and the top of the section contained virtually no diatom fossils. The most dominant species of diatom was *Planothidium delicatulum*, which occurred in large numbers (maximum: ~100% of 200) in all the 10 cm subsamples. *Planothidium delicatulum* occur in alkaline or fresh waters (Round and Bukhtiyarova 1996). The second most common species (maximum: ~190 out of 200) was *Fragilaria construens*, especially at the depths of 79.20–79.30, 79.40–79.50, and 79.90–80.00 m. The colonies of this species are not attached to the substrate, and prefer slightly alkaline water (Cejudo-Figueiras *et al.* 2011). The third most common diatom, *Cyclotella ocellata*, was found in the order of tens at depths of 79.10–79.20 m. This is a planktonic diatom species commonly found in oligotrophic lakes (Edlund *et al.* 2003). The diatom counts are provided in online supplementary material: Table S3.

3.2. Chronology of Darhad palaeolakes

3.2.1. Lake and beach sediments in Darhad basin

Insufficient sunlight under water makes it hard to fully reset the luminescence in lacustrine and fluvial sediments (e.g. Thomas *et al.* 2003; Arnold *et al.* 2007; Lüthgens *et al.* 2010) and partial bleaching was apparent in the sediments from DBC1, as shown by the large discrepancy between the ages for quartz and feldspar (Tables 1, 2, and A3) estimated by the ‘central-age’ model (Galbraith and Roberts 2012). Quartz minerals bleach more efficiently than feldspars (Wallinga *et al.* 2001),

which makes them ideal for OSL dating, but the coarse quartz grains in our samples had low sensitivity to radiation, yielding too few photons to date the samples reliably. Low sensitivity of quartz has also been observed in samples from the Gobi (Hülle *et al.* 2010) and central Mongolia (Lehmkuhl *et al.* 2011). We therefore used the minimum-age modelling (Galbraith and Roberts 2012) to estimate the D_e of feldspar grains. These gave age estimates consistent with those from quartz.

Sample DB-AG-2004-03A consisted of sand from a beach at an elevation of 1668 m asl near the Arsain river (Figure 2). Beach environments have greater sunlight exposure than lakes themselves, and bleaching there is likely to be more complete. The ages estimated from the minimum and central values of the D_e histogram and the age estimated by finite mixture modelling were statistically the same for this sample. This was not true for the deep-water or moraine samples, supporting our interpretation that the partial bleaching is common in deep-water sediments from DBC1. The sands gave a luminescence age of ~14 ka (Table 1), suggesting that at least a 120 m deep palaeolake existed at that time. The elevation of this beach is only ~10 m lower than the wave-cut benches on the MIS 2 moraines at the Jarai river (Gillespie *et al.* 2008), but ~70 m above the deeply incised outwash plains at Tengis river.

Laminated grey sandy silts at 9.15 m in DBC1 yielded a deposition age of ~20 ka (Table 1), consistent with the timing of last glacial advances at Jarai river 23 km to the northeast (Gillespie *et al.* 2008). Krivonogov *et al.* (2012) related the high concentration of sands in this layer to shoreline deposition and/or fluvial conditions, and suggested that only a shallow lake existed during this time. However, we observed that this sandy layer is not massive, but rather finely laminated suggesting calm conditions during its deposition and a deeper lake. Also, these sands were angular to subangular with low sphericity, indicating minimal transport from the source and deposition with little reworking. We infer that these sands were derived from glaciofluvial sediments when glaciers had advanced close to the range front. The relatively high magnetic susceptibility of these sediments supports our interpretation. The sandy lamina in the layer at 9.15 m alternate with silty lamina, which may indicate frequent fluctuations in lake depth, sediment supply or lake currents. The sands at 9.50 m were deposited at ~31 ka. The sediments at this depth are similar to that from the 9.15 m level, suggesting a similar glaciofluvial source. Overall, we interpret this 1 m thick sandy layer at depths of 9–10 m in the DBC1 core as evidence that a fluctuating deep palaeolake existed in Darhad basin during MIS 2. The sandy layer abruptly terminates at the depth of ~10.1 m,

Table 1. Luminescence ages for lacustrine and glacial sediments from Darhad basin.

Sample identification	Lithology	Depth (m)	Analysis type	Deposition age (ka $\pm 2\sigma$)
<i>Lake sediments from the DBC1 core, N 51.187472°, E 99.497556°, 1547 m asl</i>				
DBC1B-9.15	Fine sand	9.15	Feldspar MAM ^a	19.5 \pm 2.6
DBC1B-9.50	Fine sand	9.50	Feldspar MAM ^a	30.9 \pm 3.1
DBC1A-43.7	Fine sand	43.7	Quartz MAM ^a	34.7 \pm 8.1
DBC1A-46.8	Fine sand	46.8	Feldspar MAM ^a	45.2 \pm 9.7
DBC1A-76.9	Fine sand	76.9	Multi-mineral aliquot: OSL ^b	139.6 \pm 15.8
DBC1A-80.1	Silt	80.1	Multi-mineral aliquot: IRSL ^c	135.0 \pm 8.4
<i>Beach deposit near Arsain river, N 51.201611°, E 99.648556°, 1668 m asl</i>				
DB-AG-102504-03A	Fine sand	1.5	Feldspar MAM ^a	14.3 \pm 1.7
<i>Till from the end moraine at the Sarig valley: N 51.449861°, E 99.034278°, 1611 m asl</i>				
DB-AG-2007-002	Fine sand	~0.5	Feldspar MAM ^a	12.0 \pm 7.5

^aMAM: minimum-age model (Galbraith and Roberts 2012).^bOSL: optically stimulated luminescence (protocols of Feathers *et al.* 2012).^cIRSL: infrared stimulated luminescence (protocols of Feathers *et al.* 2012).

below which only the grey silty laminae are found, an indication to us of less energetic runoff probably because the glaciers were farther from the lake at that time.

For this study, we rejected central feldspar ages due to partial bleaching, and accepted minimum feldspar ages as reliable. Feldspar measurements had better statistics than for quartz, and the minimum feldspar ages were consistent with quartz central ages within the 2σ error. However, luminescence measurements of the sample DBC1A-43.7 (43.7 m depth) yielded only five readings from feldspar, so we accepted its minimum

Table 2. Radioactivity data for the luminescence samples. Internal K was assumed to be $12 \pm 2\%$ for all samples.

Sample identification ^a	Total dose rate (Gy ka $^{-1}$ $\pm 2\sigma$)	K (% $\pm 1\sigma$)	^{232}Th (ppm $\pm 1\sigma$)	^{238}U (ppm $\pm 1\sigma$)
DBC1B-9.15 (UW1264)	1.53 \pm 0.09	1.0 \pm 0.1 ^b	3.7 \pm 0.4	1.3 \pm 0.2
DBC1B-9.50 (UW1867)	1.29 \pm 0.06	0.92 \pm 0.03	2.3 \pm 0.5	1.2 \pm 0.1
DBC1A-43.7 (UW1265)	1.46 \pm 0.07	1.03 \pm 0.03	4.0 \pm 0.8	1.5 \pm 0.1
DBC1A-46.8 (UW1292)	1.38 \pm 0.07	0.95 \pm 0.02	5.4 \pm 0.9	1.0 \pm 0.1
DBC1A-76.9 (UW1293)	2.13 \pm 0.12	1.0 \pm 0.11	4.3 \pm 0.8	1.8 \pm 0.1
DBC1A-80.1 (UW2702)	3.30 \pm 0.16	1.64 \pm 0.11	9.8 \pm 1.3	1.9 \pm 0.2
DB-AG-2004-03A (UW1868)	1.63 \pm 0.08	1.02 \pm 0.02	5.6 \pm 0.8	0.8 \pm 0.1
DB-AG-2007-002 (UW1872)	1.79 \pm 0.11	1.28 \pm 0.09	3.3 \pm 0.7	0.9 \pm 0.1

^aUniversity of Washington laboratory numbers are given in the parentheses.^bAssumed concentration. The measured concentration of K in sample DBC1B-9.15 was too high, probably due to machine error, and we assumed a value of 1.0 ± 0.1 , similar to the other samples.

quartz age of 34.7 ± 8.1 ka ($n = 21$) as the sample age. Fine sands from 46.8 m in the DBC1 core yielded a deposition age of 45.2 ± 9.7 ka. A significant increase in the magnetic susceptibility suggests that these sands were derived mostly from runoff sediments. We note that the error for these MIS 3 samples is relatively high (>20%) relative to the younger samples, which prevents estimating the sedimentation rates accurately for this time period. The two new peat samples from the Shargyn river cutbank (Figure 2) yielded ^{14}C ages of ~46 and 48 ^{14}C ka BP (Table 3), which were beyond

Table 3. ^{14}C samples and data.

Sample ID	Lab number	Material	Depth (cm)	Fraction modern	D ₁₄	^{14}C age (^{14}C year BP $\pm 1\sigma$)	Corrected ^{14}C ages (^{14}C year BP $\pm 1\sigma$)	Calibrated age (cal year BP $\pm 2\sigma$)
Sentsa river, eroded cliff of thermokarst lake, N 52.665850°, E 99.489833°, 1326 m asl								
071002-Rsna-01	97499	Charcoal	12–20	0.9377 \pm 0.0043	-62.3 \pm 4.3	515 \pm 40	515 \pm 40	500–560
071002-Rsna-02	97500	Sedge blade	60	0.4442 \pm 0.0021	-555.8 \pm 2.1	6520 \pm 40	6520 \pm 40	7410–7510
071002-Rsna-03	97501	Plant remains	73	0.8117 \pm 0.0036	-188.3 \pm 3.6	1675 \pm 40	1675 \pm 40	1520–1700
071002-Rsna-04	97502	Plant remains	195	0.4630 \pm 0.0025	-537 \pm 2.5	6185 \pm 45	6185 \pm 45	6950–7180
071002-Rsna-05	97503	Wood	172	0.7767 \pm 0.0034	-223.3 \pm 3.4	2030 \pm 40	2030 \pm 40	1890–2070
Oka river, cross-bedded sand from ice marginal lake, N 52.315567°, E 100.113133°, 1469 m asl								
071202-Roka-04	97504	Wood	3.2	0.2212 \pm 0.0011	-778.8 \pm 1.1	12,120 \pm 40	12,120 \pm 40	13,820–14,130
071202-Roka-05	97505	Wood	4.3	0.2141 \pm 0.0011	-785.9 \pm 1.1	12,380 \pm 45	12,380 \pm 45	14,140–14,740
Batig river, aeolian sands capping the Darhad palaeolake sediments, N 51.039633°, E 99.400283°, 1559 m asl								
061802-ag-DB-02	97357	Woody roots	0.1	0.6378 \pm 0.0029	-366.3 \pm 2.9	3615 \pm 40	3615 \pm 40	3830–4000
061802-ag-DB-01	97358	Peat	0.1	0.5847 \pm 0.0026	-419.1 \pm 2.6	4310 \pm 40	3810 \pm 40	4090–4300
Arsain river, archaeological site formed after the Darhad palaeolake dried, N 51.281650°, E 99.690733°, 1559 m asl								
061902-ag-AG-11	97359	Charcoal	~0.5	0.7486 \pm 0.0034	-256.2 \pm 3.4	2325 \pm 40	2325 \pm 40	2300–2460
Shargyn river, cutbank exposing the Darhad palaeolake sediments, N 51.428433°, E 99.702400°, 1558 m asl								
062002-ag-JG-02	97360	Peat	~8.1	0.0023 \pm 0.0006	-997.7 \pm 0.6	48,890 \pm 2230	48390 \pm 2230	>47500
062002-ag-JG-03	97361	Peat	~7.8	0.0028 \pm 0.0006	-997.3 \pm 0.6	47,340 \pm 1840	46840 \pm 1840	>47500

Analyses performed at Center for Acceleration Mass Spectrometry (CAMS), Lawrence Livermore National Laboratory. $\delta^{13}\text{C}$ values of -25‰ were assumed according to Stuiver and Polach (1977) when given without decimal places. Values measured for the material itself are given with a single decimal place. Radiocarbon concentrations are given as fraction modern and D₁₄C. Ages are calculated using the Libby half-life of 5568 years and following the conventions of Stuiver and Polach (1977). Sample preparation backgrounds have been subtracted, based on measurements of samples of ^{14}C -free coal or calcite. Backgrounds were scaled relative to sample size. ^{14}C ages for peat were corrected for reservoir effect of 500 ^{14}C years, a value observed in disseminated organic carbon in the Hövsgöl lake (Gillespie *et al.* 2008). 2 σ range calculated using CALIB version 7.1 (Stuiver and Reimer 1993) and IntCal13 calibration curve (Reimer *et al.* 2013), and rounded to nearest decade.

Table 4. ^{10}Be ages for samples from Mönh Saridag peak, East Sayan and Hangai mountains, Hoit Aguy massif, and the Tengis end moraine at the Sarig river valley.

Sample identification	Sample description	Maximum diameter (m)	Exposure age ^a (ka $\pm 1\sigma$)	Internal uncertainty (1 σ)
Mönh Saridag, left-lateral moraine, N 51.736086°, E 100.599854°, 2640 m asl				
070402-AG-RMS-1	Quartz vein boulder	1.0	12.3 \pm 0.9	0.6
070402-AG-RMS-2	Red granite boulder	1.5	12.3 \pm 0.8	0.4
Mönh Saridag, medial moraine, N 51.730918°, E 100.600732°, 2800 m asl				
070402-AG-RMS-3	Granodiorite boulder	1.5	10.7 \pm 0.7	0.4
070402-AG-RMS-4	Granodiorite boulder	4.0	10.4 \pm 0.8	0.4
070402-AG-RMS-5	Quartz vein in pegmatite	2.0	9.7 \pm 0.7	0.6
Mönh Saridag, left-lateral moraine, N 51.728600°, E 100.598324°, 2900 m asl				
070402-AG-RMS-6	Granodiorite boulder	2.0	1.5 \pm 0.1	0.1
070402-AG-RMS-7	Quartz boulder	1.5	1.2 \pm 0.1	0.1
Mönh Saridag, end moraine, N 51.738667°, E 100.600855°, 2640 m asl				
070402-AG-RMS-8A	Quartz vein	1.0	26.4 \pm 1.7	0.8
070402-AG-RMS-8B	Quartz vein	1.0	20.1 \pm 1.3	0.6
070402-AG-RMS-9	Quartz vein in granodiorite	2.0	28.4 \pm 1.8	0.8
Sailag river, broad left lateral–end moraine, N 52.788700°, E 99.736472°, 1454 m asl				
070802-AG-RSLK-1	Granite boulder	4.0	20.9 \pm 1.5	0.9
070802-AG-RSLK-2	Red granite boulder	1.5	22.7 \pm 1.6	1.0
070802-AG-RSLK-3	Red granite boulder	1.2	20.6 \pm 1.4	0.9
070802-AG-RSLK-4	Red granite boulder	2.0	64.4 \pm 4.3	2.3
070802-AG-RSLK-5	Red granite boulder	2.0	20.0 \pm 1.4	0.9
Sailag river, stagnant ice terrain on the fan, N 52.784657°, E 99.732189°, 1410 m asl				
070802-AG-RSLK-6	Red granite boulder	1.0	14.1 \pm 1.0	0.6
070802-AG-RSLK-7	Diorite boulder	1.0	16.5 \pm 1.1	0.6
070802-AG-RSLK-8	Granodiorite boulder	1.5	12.4 \pm 1.3	1.1
070802-AG-RSLK-10	Red granite boulder	1.5	18.7 \pm 1.3	0.8
Jombolok river, end moraine, N 52.731073°, E 99.615047°, 1410 m asl				
071002-AG-RDJO-1	Granodiorite boulder	1.5	19.8 \pm 1.4	0.9
071002-AG-RDJO-2	Granodiorite boulder	1.0	20.8 \pm 1.5	0.9
071002-AG-RDJO-3	Granite boulder	1.0	34.5 \pm 3.0	2.3
071002-AG-RDJO-5	Granodiorite boulder	0.8	23.0 \pm 2.1	1.6
Jombolok river, right-lateral moraine, N 52.717833°, E 99.599533°, 1392 m asl				
071002-AG-RDJO-6	Granodiorite boulder	6.0	18.8 \pm 1.3	0.7
Oka river, broad end moraine, N 52.298633°, E 100.224617°, 1518 m asl				
071202-AG-ROKA-6	Meta-granodiorite /gneiss	0.6	16.1 \pm 1.2	0.8
Gyalgar peak, left-lateral moraine in the trunk valley, N 48.183767°, E 98.781450°, 2472 m asl				
ZAG-ARG-01A	Granitic boulder	6.0	24.4 \pm 1.6	0.7
ZAG-ARG-01B	Granitic boulder	-	20.2 \pm 1.3	0.5
Gyalgar peak, end moraine in the trunk valley, N 48.1200°, E 98.813417°, 2285 m asl				
ZAG-ARG-02B	Granitic boulder	1.5	17.2 \pm 1.2	0.5
Gyalgar peak, end moraine in the trunk valley, N 48.118050°, E 98.815833°, 2253 m asl				
ZAG-ARG-03A	Pink granitic boulder	1.0	22.6 \pm 1.8	1.0
ZAG-ARG-03B	Granitic boulder	1.2	158.3 \pm 11.4	5.2
Gyalgar peak, right-lateral moraine in the trunk valley, N 48.129017°, E 98.798217°, 2352 m asl				
ZAG-ARG-04B	Granitic boulder	0.3	27.6 \pm 1.8	0.7
Gyalgar peak, left-lateral moraine in the side valley, N 48.182884°, E 98.804676°, 2585 m asl				
ZAG-SB-04A	Granitic boulder	-	30.0 \pm 1.9	0.6
ZAG-SB-04B	Granitic boulder	-	58.5 \pm 3.5	0.8
ZAG-SB-04C	Granitic boulder	-	24.5 \pm 1.5	0.5
Gyalgar peak, bedrock above the side valley, N 48.195113°, E 98.792166°, 2815 m asl				
ZAG-SB-05	Granitic boulder	-	158.1 \pm 9.8	2.1
Hoit Aguy massif, right-lateral moraine, N 51.552057°, E 98.714686°, 2335 m asl				
080709-HA-JB-02	Granitic boulder	0.3	36.1 \pm 2.3	1.1
080709-HA-JB-03	Granitic boulder	0.8	34.0 \pm 2.5	1.7
Sarig valley, end moraine of the Tengis glacier, N 51.453579°, E 99.038698°, 1631 m asl				
150707-DB-AG-003A	Pink granitic boulder	1.5	23.8 \pm 1.5	0.7
150707-DB-AG-003C	Red granitic boulder	1.5	20.7 \pm 1.4	0.7
Jarai pass, boulders on the N 51.595383°, E 99.986200°, 2459 m asl				
6-25-02-ag-JG01a	Red granitic boulder	1.5	43.8 \pm 9.9	9.5
6-25-02-ag-JG01b	Granitic boulder	1.5	18.3 \pm 1.3	0.8
Jarai pass, bedrock, N 51.595383°, E 99.986200°, 2459 m asl				
6-25-02-ag-JG01c	Quartz vein in schist	1.0 ^b	15.0 \pm 1.1	0.7

^aExposure age includes total uncertainty, compounded from random errors in measuring the Be concentration (internal uncertainty), and from systematic errors arising from modelling the production rate of Be rate due to nuclear spallation and due to muons.

^b1-cm quartz vein on upper surface of a 1-m schist erratic boulder on bedrock.

the limit of the IntCal13 calibration curve (Reimer *et al.* 2013). Nonetheless, these ages for the lake sediments recovered from the DBC1 and Shargyn river cutbank

support the findings of Gillespie *et al.* (2008) that Darhad basin hosted a deep lake at least intermittently (53–35 ka) during MIS 3.

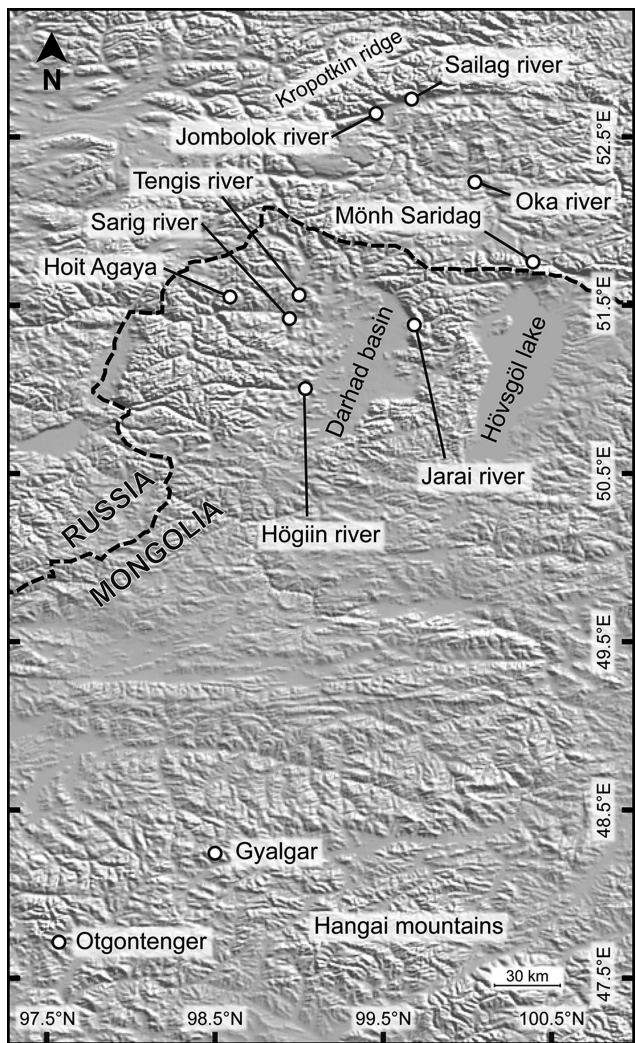


Figure 3. CRE dating sites: Index map showing Sayan, Hoit Aguy, Darhad, Hangai sites: SRTM shaded-relief image showing the locations of the 99 ^{10}Be sampling sites referred to in this study. Gillespie *et al.* (2008) sampled 22 boulders in Darhad basin. Rother *et al.* (2014) sampled 21 boulders in the Otgontenger mountain. Arzhannikov *et al.* (2012) dated moraines at the Jombolok and Sailag rivers (13 samples).

There is a massive sandy layer at a depth of 76.9 m. The low magnetic susceptibility of the sands in this 0.65 m thick layer and their unconformable contact with the deep-water lake sediments suggest that these were reworked sands deposited in a shallow lake. The sand fractions in the sample DBC1A-76.9 was insensitive to green-laser stimulation, but fine-grained multi-mineral aliquots prepared from the same sample gave an OSL age of 126.5 ± 19.8 ka and an IRSL age of 162.8 ± 26.4 ka (Table A3), which overlap each other at the 2σ level. In this case, we calculated the weighted average for the estimated age at 139.6 ± 15.8 ka for DBC1A-76.9. A silt-dominated layer abruptly interrupts the sands at 77.6 m and continues until ~79 m depth.

Below the silt there is the unique 1 m carbonate layer. Mollusc shells are abundant and embedded within the thin laminations of this section, suggesting a very shallow lake, probably in an interglacial climate. Batbaatar *et al.* (2012) found sponge spicules and stratospores in the carbonate layer, probably an indication of a palaeolake with restricted environment and summer desiccation from a seasonally dry climate.

There were no clastics in the carbonate layer suitable for dating; therefore, we subsampled and dated the underlying silts from 80.1 m depth. The OSL measurements of the sample DBC1A-80.1 underestimated the age, possibly due to saturation effects in the quartz grains (Feathers and Pagonis 2015). We accepted the IRSL age of 135.0 ± 8.4 ka for DBC1A-80.1. However, we note that the accepted ages for the samples DBC1A-76.9 and DBC1A-80.1 are not precise, overlapping within the 2σ error, and we could not definitely constrain the maximum ages for both samples.

3.2.2. End moraine of the Tengis glacier

The end moraine in the Sarig valley, 1 km south of the Maly Yenisei river, is perhaps the most convincing evidence to support that the Tengis glacier crossed the river and impounded a lake in Darhad basin (Figures 2 and 5). We dated two granitic boulders there, yielding exposure ages of ~21 and ~24 ka that overlap within 2σ uncertainty (Table 4). The MIS 2 age for the terminal moraine of the Tengis glacier is consistent with the results of Gillespie *et al.* (2008) that the glaciers around Darhad basin were large and extended to the basin floor during MIS 2. The luminescence ages for the sandy layers at ~9 m depth in the DBC1 core suggest the existence of a deep MIS 2 lake in Darhad basin, which further support the conclusion of Gillespie *et al.* (2008) that the latest Tengis glacier to impound the Maly Yenisei was during the global LGM.

We attempted to date the moraine tills in the Sarig valley directly, using luminescence dating. The quartz grains were insensitive to the light stimulation and yielded very few signals. The feldspars were much better in yielding signals, but the equivalent doses varied significantly, probably because the existing luminescence signals were not properly reset due to incomplete exposure to sunlight. Therefore, we used the minimum age model of Galbraith and Roberts (2012), which estimated the minimum age at ~12 ka with a large error of ± 7.5 ka (2σ ; Table 1).

3.2.3. Surface sediments from Darhad basin

We sampled the surface sediments overlying the lake sediments in Darhad basin to constrain the time when the basin was completely drained and started to resemble

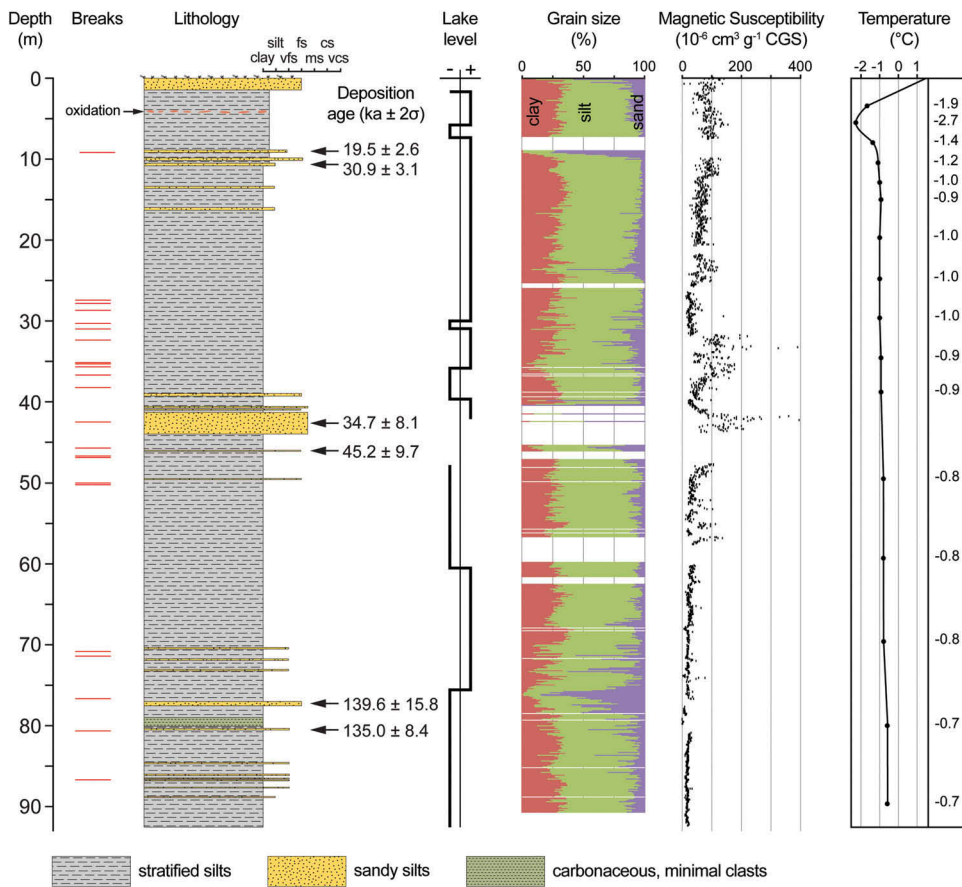


Figure 4. Stratigraphic column of the DBC1 core. Sand and silts from the core used for luminescence dating. Lake level was inferred from the facies by Andrei Fedotov, Limnological Institute, Siberian Branch, Russian Academy of Sciences (2008 personal communication). Magnetic susceptibility was measured in the field, and re-measured in the laboratory using Bartington reader MS2B. Grain size was measured at the Institute of Petroleum Geology and Geophysics, SB RAS, using Microtrac X100 and Microtrac ASVR. Temperature of the borehole was measured by conventional thermometry. Colour version is available online.

its modern condition. The Batig river (Figure 2) flows through a nearly flat plain near the centre of the basin and exposes an outcrop of aeolian sands capping the lake sediments. Two samples of wood and peat there yielded calibrated ^{14}C ages of ~3.9 and 4.1 cal ka BP. We also found an archaeological site near the Arsain river that was littered with broken pieces of animal bones and the remains from a fireplace. The charcoal sample from this site yielded a ^{14}C age of ~2.3 cal ka BP. These ages suggest that the last of the shallow Darhad palaeolakes was drained by ~4 ka, and probably the basin has remained largely dry since then. Consistent with this interpretation, Ishikawa and Yamkhin (2015) found that the permafrost pingo near the Arsain river started forming after ~4.5 ka.

3.3. Glacial chronology in the vicinity of Darhad basin

3.3.1. East Sayan ice field

The Jombolok river valley was occupied by an outlet glacier from Kropotkin ridge in the East Sayan ice field.

Its end moraine is located ~2 km up-valley from an MIS 3 buried soil dated to 38,380–43,860 cal year BP by Arzhannikov *et al.* (2012). We sampled four boulders sitting on the end moraine (Figure 6(d)). One sample was older and appeared to have inherited ^{10}Be , but the average age for the other three was ~21 ka. Down-valley from this moraine ~2 and 6 km are two sets of end moraines that Arzhannikov *et al.* (2012) dated to ~26 and 25 ka, respectively (recalculated ages: Batbaatar and Gillespie 2015). The ^{10}Be ages for these two end moraines correspond to standstills or minor re-advances of the Jombolok outlet glacier during MIS 2. We also dated a boulder from a right-lateral moraine of the same outlet glacier at ~19 ka.

Another outlet glacier from the East Sayan ice field descended the Sentsa river valley before ultimately merging with the Jombolok river valley. Arzhannikov *et al.* (2012) sampled boulders on the left-lateral moraines and dated them to ~19 ka. At the bank of a thermokarst lake, Vasil'chuk *et al.* (2015) dated the oldest sediments at ~7 cal ka BP. We examined the eroded cliff of another

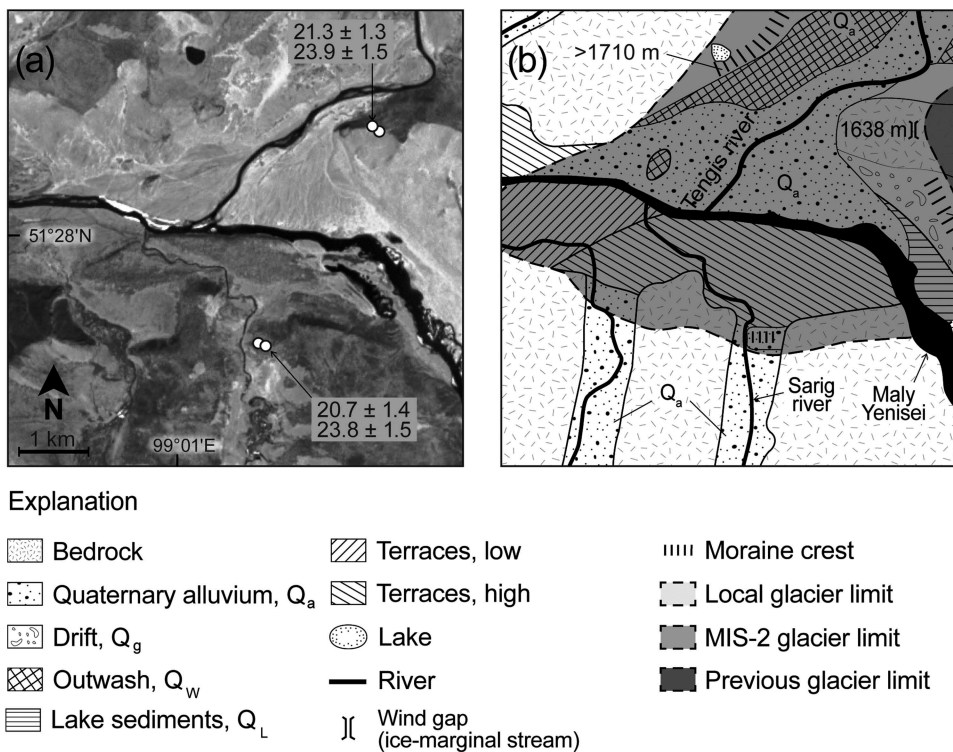


Figure 5. CRE sampling site of the end moraine of the Tengis glacier. (a) ASTER band 3N showing the end moraine in the Sarig river valley and the confluence of Tengis river to the Maly Yenisei. The ages for the boulders on the wind gap are from Gillespie *et al.* (2008). Ages are in $\text{ka} \pm 1\sigma$; (b) Generalized map of the same area as in (a), from Gillespie *et al.* (2008).

thermokarst lake in the valley, 500 m west of this site, to determine the minimum ages for the glacial retreat, sampling organic materials stratigraphically overlying the glacial deposits. The oldest plant remains from the ~2 m depth dated to ~7 cal ka BP. Two of the ^{14}C ages don't agree stratigraphically, probably due to carbon contamination from other sources. The charcoal sample at the top underlies the loess sediments capping the stratigraphy and was dated to ~0.5 cal ka BP. The ^{14}C Sentsa ages therefore provide only loose constraints for the end of the last glaciation there.

The Sailag river merges with the Jombolok river from the northwest, and the glaciers there originated from the local peaks, rather than from a distant ice field. This simplicity makes the estimation of local ELA easier and more reliable, and therefore is important to establish a robust chronology of glacial advances there. The average age for the four boulders (Figure 6(b,c)) collected from the stagnant-ice terrain at elevation 1454 m asl was ~15 ka. A few metres higher in this terrain, the left-lateral moraine yielded an age of ~21 ka averaged from four samples (excluding RSLK-4: ~64 ka). The ages are consistent with the ~18 ka age that Arzhannikov *et al.* (2012) measured for two boulders from the right-lateral moraine in the same valley. The estimated ELA for this

MIS 2 advance is ~2020–2100 m asl (THAR = 0.58, Gillespie *et al.* 2008).

The Oka river hosted outlet glaciers from the East Sayan ice field, as shown by lateral and recessional moraines found along the river. We dated a single boulder, ~16 ka, sitting on a recessional moraine at ~1510 m asl (Figure 6(e)). Numerous lakes, reversed and crossing drainages, and nunataks in the surrounding Sayan mountains suggest that a vast ice field covered the uplands down to ~2050 m asl there (Figure 4 in Batbaatar and Gillespie 2015). Our sample represents a time when the outlet glaciers from the East Sayan ice field had retreated from their maximum extents of MIS 2.

Mönh Saridag (3491 m asl) is the highest peak of the East Sayan mountains. In a cirque on its northern side is a series of moraines leading up to the modern Peretolchin glacier at ~2930–3270 m asl. We sampled 10 boulders from the moraine crests there (Figure 7(a)). Three boulders from the lowest moraine of the series, on a bedrock ridge impounding a tarn at ~2620 m asl, gave an average age of ~25 ka, consistent with the MIS 2 glacier advance recorded elsewhere in the East Sayan mountains. These three ages suggest that by 25 ka the MIS 2 glaciers had already retreated to the lip of the cirque. Up-valley ~400 m, a higher moraine dated to

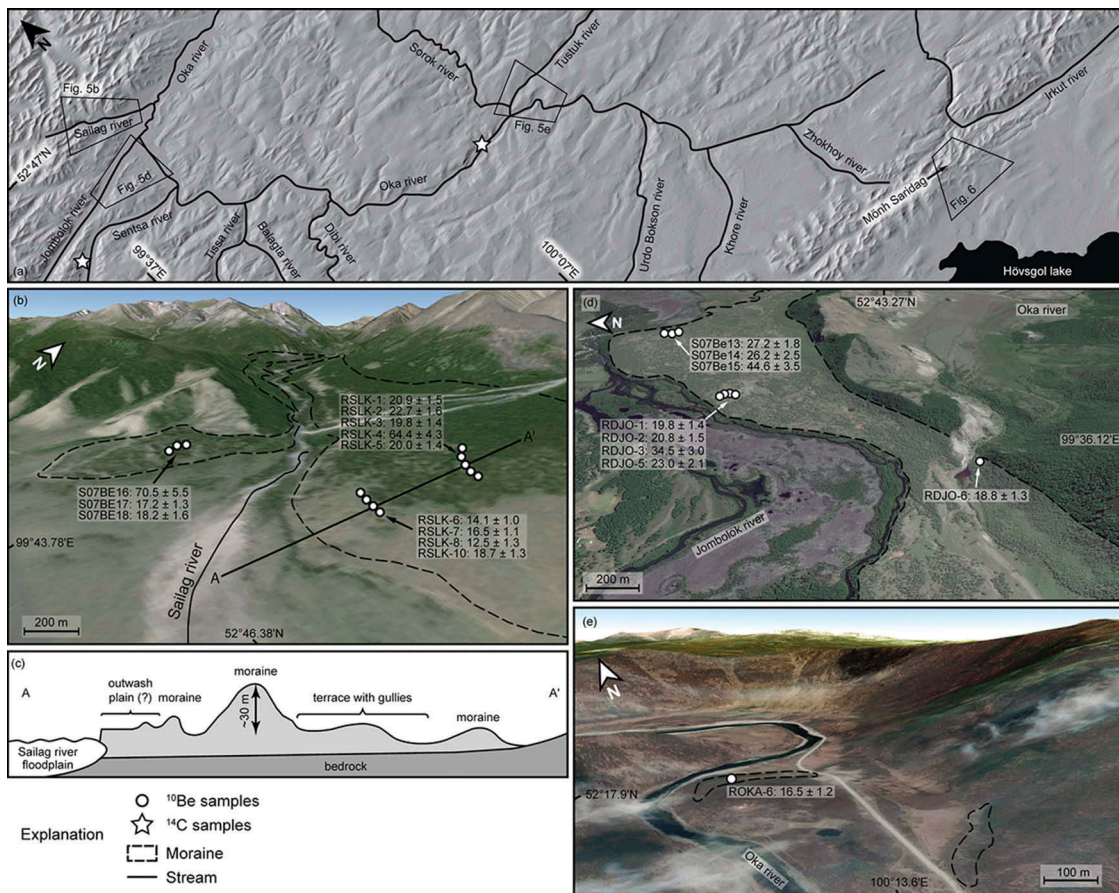


Figure 6. East Sayan sampling sites: (a) Shaded-relief image showing major tributaries to the Oka river. Stars indicate ^{14}C sampling sites at the Sentsa and Oka rivers; (b) Google Earth perspective view of the Sailag river valley (overlay image: Landsat TM); (c) Sketch profile across the sampled moraine. Distance not to scale; (d) Google Earth perspective view of the Jombolok river valley and the CRE sample locations (overlay image: DigitalGlobe); (e) Google Earth perspective view of the Oka river valley and the CRE sample location (overlay image: DigitalGlobe). Samples labelled S07Be are from Arzhannikov *et al.* (2012). Ages are in ka $\pm 1\sigma$. Colour version is available online.

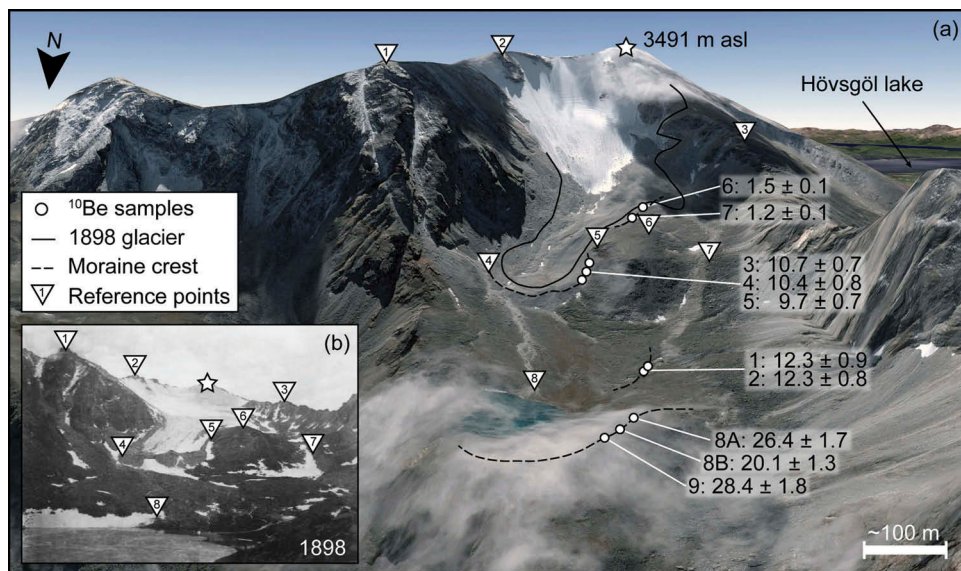


Figure 7. CRE sampling site at the Mönkh Saridag mountain. (a) Google Earth perspective view showing the modern glacier Peretolchin, and CRE sample locations on moraine crests (overlay image: DigitalGlobe); (b) Photo taken in 1898 of the Peretolchin glacier (Peretolchin 1908). We used more reference points than shown in the figure to visually match the landscape features in Google Earth image and the photograph. All sample numbers refer to 070402-AG-RMS- as listed in Table 4. Ages are given in ka $\pm 1\sigma$. Colour version is available online.

~12 ka ($n = 2$) suggests further gradual episodic retreat or retreat and re-advance. Three boulders from a recessional moraine even further up-valley at ~2800 m asl were dated at ~10 ka, consistent with continued gradual retreat. The highest of the dated end moraines is at ~2900 m asl, ~300 m from the modern ice tongue. Two boulders from this moraine dated at ~1.3 ka. The Peretolchin glacier in 1898 (Peretolchin 1908) was very close to this late neoglacial moraine. Our visual matching of the 1898 photo and Google Earth (Figure 7(b)) suggests that the 1898 glacier advance did not overrun the older moraines we dated.

3.3.2. Bayan Zürhiin ranges

To the east of Darhad basin, the Bayan Zürhiin ranges were another centre of glaciation. The wide U-shaped valleys of the Utragiin, Jarai, Jumarlag, and Hodon rivers (Figure 2) contain end moraines and hummocky terrain at the edge of Darhad basin. Gillespie *et al.* (2008) dated the sequence of end moraines at the mouth of the Jarai river valley to ~40 and ~22 ka, establishing the chronology for the largest extents of glaciers there. However, the timing of the glacial retreat is unknown. To address this problem, we sampled two glacial boulders and one glacially eroded bedrock at the head of the Jarai river (Figure 8). The site marks a pass between Darhad and Hövsgöl basins. There are red granitic erratics resting on the local schist bedrock of the pass. Numerous tarns on the flat, glaciated upland between Jarai pass and the Ih Horoo valley to its north indicate the presence of a local ice cap between the drainages (Batbaatar and Gillespie 2015). The Ih Horoo valley was last glaciated during MIS 2 (Wegmann *et al.* 2011), and that is likely the age of the

ice cap also. The erratics on the pass were likely deposited when the flux of ice south of the pass ended.

Two granitic boulders on Jarai pass dated to ~44 and 18 ka, and quartz from a lens in the schist bedrock dated to ~15 ka. Assuming that the oldest sample was exposed before the glacial transport and thus contained inherited ^{10}Be , we conclude that the Jarai glacier had retreated all the way to the cirques by ~15 ka and the Bayan Zürhiin ranges became largely ice-free by then. This is a few thousand years after the MIS 2 glacier at Mönh Saridag retreated to its cirque. The time frame for the glacier retreat from the Bayan Zürhiin ranges, 15–18 ka, coincides with the timing of the retreat of outlet glaciers in the Jombolok, Oka, and Sailag river valleys.

3.3.3. Hoit Aguy massif

At their maximum extents, some of the valley glaciers in the Hoit Aguy massif joined the outlet glaciers descending from the East Sayan ice field. The terminal moraines in other valleys of the Hoit Aguy sit above the main outlet glacier. We sampled two boulders from a right-lateral moraine extending into a terminal moraine that lies ~50 m above the trunk outlet trimlines at ~2030 m asl there (Figure 9). The lateral moraine was dated to ~35 ka, suggesting an MIS 3 advance at the Hoit Aguy massif with an ELA of ~2330 m asl (MELM). Elevated hummocky terrain between the valleys suggests that the valley glaciers of the Hoit Aguy massif were not always individually separated and constrained within their valleys. This means that larger glaciers existed there once and must have been part of the East Sayan ice field. The terminal moraines impounding the modern paternoster lakes of Hoit Aguy massif sit very close and are interior to the MIS 3 moraines. The ELA for these smaller moraines is only 50 m above the MIS 3 advance. This is consistent with the pattern of ELA for the MIS 2 and 3 moraines dated in Darhad basin (Gillespie *et al.* 2008).

3.3.4. Hangai massif in central Mongolia

The Hangai mountains of central Mongolia, a centre of extensive glaciations separate from the Siberian glaciers, provide an excellent location at which to understand the regional pattern of glacial extents better. We analysed 10 samples from a formerly glaciated valley near Gyalgar peak (Figures 3 and 10), nine of which were from the moraines and one of which was from a bedrock outcrop above the highest lateral moraines there. Two of the ages significantly disagreed with the other ^{10}Be ages, at ~158 and ~59 ka, probably due to inherited ^{10}Be . The remaining seven ages scattered from 17.2 to 30 ka, and the average age for these moraines at ~24 ka suggests that the maximum glaciation there

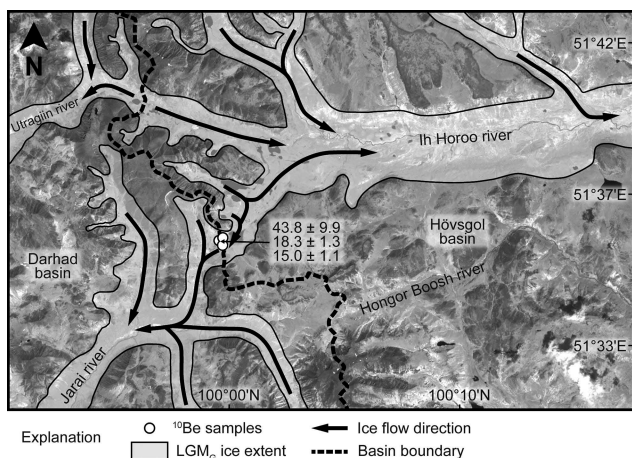


Figure 8. CRE sampling site at the pass between Darhad and Hövsgöl basins. The background image is ASTER band 3N. The ice extent is adapted from Batbaatar and Gillespie (2015). Ages are in ka $\pm 1\sigma$.

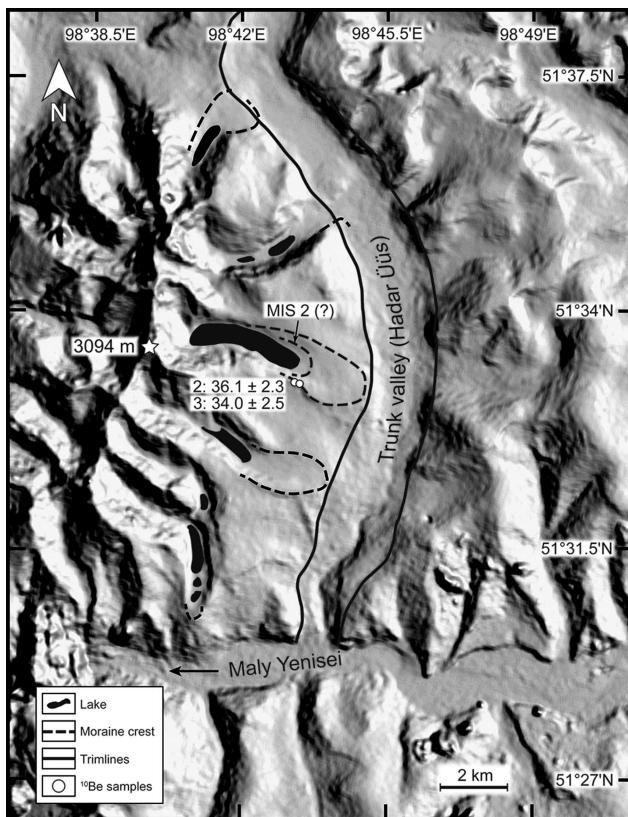


Figure 9. Hoit Aguy moraine map: Shaded-relief image of the Hoit Aguy massif and ^{10}Be sample location. Sample numbers refer to 080709-HA-JB- in Table 4. Ages are in ka $\pm 1\sigma$. Palaeoglaciers in the main trunk valley (Hadar Üüs river) originated from the East Sayan ice cap. The MIS 3, and LGM_G moraines in the Hoit Aguy hang above the trimlines of the larger glacier in the trunk valley.

coincided with the MIS 2 glaciers of Darhad basin and the East Sayan mountains.

The outlet glaciers near Otgontenger peak, another glaciated centre in the Hangai mountains, showed a similar timing of the maximum glaciations – the local LGM occurred during MIS 3 but the MIS 2 glaciers were nearly as large (Rother *et al.* 2014) as also occurred in Darhad basin.

3.4. Equilibrium-line altitude estimations

According to Gillespie *et al.* (2003, 2008) Darhad basin and the adjacent area belongs in a region where MIS 2 and earlier MIS 3 glaciers were similar in size and ELA. Modelling by Rupper *et al.* (2009) suggested that the glaciers in this region respond strongly to changes in temperature, which varies spatially much less than precipitation in Central Asia. Accordingly, we expect MIS 3–MIS 2 ELA changes to be consistent across the region. In this section, we first describe the modern ELA pattern in the regions

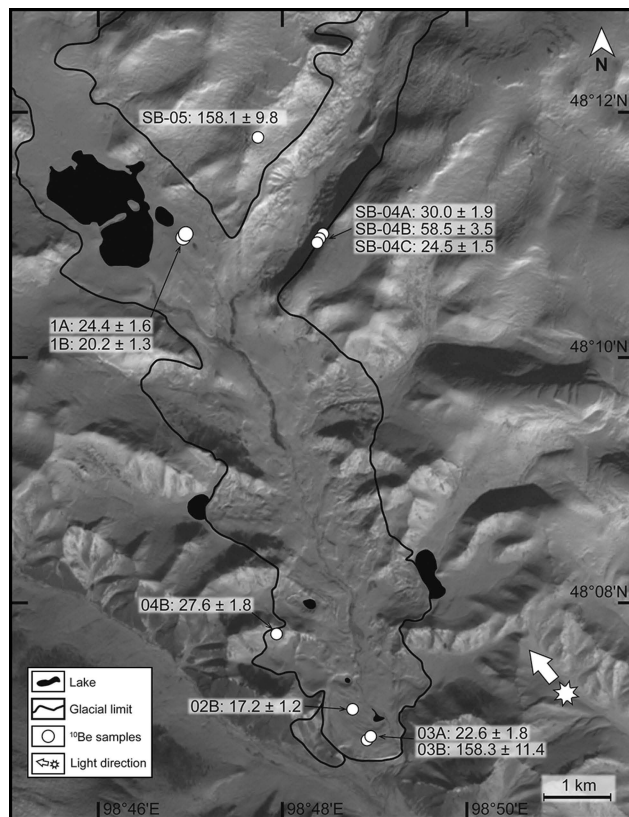


Figure 10. ASTER 3N image (acquisition: 7 January 2007) showing the Gyalgar mountain area and the CRE sample locations. All the sample numbers refer to ZAG-ARG- as listed in Table 4, except SB- is for ZAG-SB- in the table. Ages are in ka $\pm 1\sigma$.

adjacent to Darhad basin within ~1000 km, an arbitrarily chosen radius, where more than 60% of the annual precipitation falls in summer and the glaciers have a similar accumulation regime (Sakai *et al.* 2015). Then, we present the palaeo-ELA estimations for the dated moraines to compare with the modern values. In order to explain the climate conditions in the region, we compared the regional temperature and precipitation from 1901 to 1931, compiled from the interpolated climate data set CRU TS3.10 (Harris *et al.* 2014).

3.4.1. Modern glaciers and ice caps

Today only a few peaks within 500 km from Darhad basin host small cirque glaciers and ice caps: Mönh Saridag, Topografov, and Grandiozny in the East Sayan (.kmz file: online supplementary material), and Otgontenger in the Hangai mountains (Figure 3). The ELA of a small cirque glacier at the Grandiozny peak is ~2250 m asl, a low elevation consistent with colder climate of the high latitude. The ELA increases to the south, to ~2520–2680 m asl at Topografov peak and ~3190 m asl at Mönh Saridag. Approximately 500 km farther south, the ice cap on the Ogtontenger peak has

an ELA of ~3840 m asl, which reflects an increased ELA due to warmer climate at its lower latitude.

The correlation between the increasing ELA and the decreasing latitude is more pronounced when we include modern glaciers located within ~1000 km radius from Darhad basin. These are the glaciers in the Altai mountains in the west, the eastern Tien Shan in the southeast, and the Transbaikalian mountains in the northeast. The mountain ranges in this region receives at least 50% of the precipitation in summer and, in general, the annual precipitation increases from ~100 mm at 45° N to ~600 m at 55° N. The long-term (1901–1931) summer (JJAS) temperature decreases from ~10°C to ~5°C from latitude 40° N to 55° N, which corresponds to the increased ELA in the colder climates. The modern ELA of glaciers within ~1000 km from Darhad basin is lowered by ~150 m per degree of increase in latitude (see details in online supplementary material).

3.4.2. Palaeoglaciers in the vicinity of Darhad basin

The THAR ELA for the Tengis end moraine that dated to MIS 2 was ~2100 m asl, and that for the highest lateral moraine was ~2200 m asl (Gillespie *et al.* 2008). Similarly, the end moraine (?) of the MIS 2 glaciers in the Arsain river valley implied an ELA of ~2160 m asl, and the adjacent Jarai valley had a THAR ELA of 2065 m asl (MIS 2), but also received ice from the ice cap between the Jarai and Ih Horoo glaciers (Gillespie *et al.* 2008). The glaciers from the Kropotkin ridge (Figure 3) that filled the Jombolok river valley during MIS 2 had a THAR ELA was ~2120 m asl. The simple geometry of the Sailag river valley allowed a more confident THAR ELA determination for the MIS 2 moraines there of ~2050 m asl. The exception among the dated moraines in the East Sayan mountains was the MIS 2 glacier of Mönkh Saridag with an ELA of ~3000 m asl, but this glacier was in retreat.

The ELA for the dated Hoit Aguy MIS 3 moraine was ~2240 m asl (THAR) or ~2330 m asl (MELM), roughly 150 m higher than for glaciers from the main part of the East Sayan. The Hoit Aguy massif is oriented roughly N–S, and we speculate that the ridge blocks the westerlies and places the east-side drainages in a rain shadow, raising the ELAs there. The lowest end moraines on the western valleys give the THAR ELAs of 2110–2190 m asl, which was ~100 m lower than for the lowest end moraines on the eastern valleys. In addition, we found that the THAR ELA we estimated for valleys with multiple cirques was consistently lower (by ~100 m) than for valleys with a single cirque, likely because the accumulation area in the former was

greater. An inset moraine (MIS 2?) is ~700 m up-valley from the dated MIS 3 moraine, giving an estimated THAR ELA of ~2290 m asl there. After adjusting for the rain-shadow effect (2190 m asl) and variation in accumulation area differences (2090 m asl), it appears that the ELAs for the Hoit Aguy and East Sayan are about the same.

We may also compare the MELM ELAs: In the dated valley in the Hoit Aguy, the MELM ELA corrected for the rain-shadow effect is ~2230 m asl (MIS 3) or ~2280 m asl (MIS 2), ~80 m higher than the MELM ELA of ~2200 m asl for the MIS 2 Tengis glacier. This is within the ELA estimation error of 100 m.

The end moraines of the MIS 2 Gyalgar glacier in the Hangai massif implied a THAR ELA of ~2650 m asl. This is similar to the THAR ELA for the MIS 2 end moraines of the Ongontenger glacier reported by Rother *et al.* (2014). The elevation of the highest lateral moraine there was ~2750 m asl, only ~100 m above the THAR ELA. Similar to the modern ELA pattern in the vicinity of Darhad basin, the ELAs for the MIS 2 glaciers were also lower in the East Sayan than in the Hangai. The difference of ~500 m between the MIS 2 ELAs of the East Sayan and the Hangai suggest that the MIS 2 ELA varied by ~130 m per degree of latitude.

4. Discussion

We expect that the ^{10}Be ages from Darhad basin and the corresponding ELAs for the local maximum glacial (LGM_l) advances should correlate well with the glaciations in the adjacent areas based on four reasons: (1) the seasonality of precipitation is similar, hence the glacier accumulation regime is likely similar also (e.g. Sakai *et al.* 2015; online supplementary material); (2) the modern ELAs show a consistent pattern of smooth variation, changing only with latitude; (3) the sensitivity of glaciers in the region is expected to be similar (e.g. Rupper and Roe 2008) because they are mostly controlled by changes in temperature, which is less spatially heterogeneous than precipitation; (4) general circulation models show that both precipitation and temperature exhibited low variability during MIS 2 in northern Mongolia (e.g. Rupper and Koppes 2010), suggesting that the amplitude of climate forcing was similar from place to place.

A large number (67) of ^{10}Be ages for glacial deposits, at least 2–5 per moraine, has now been determined for the southern and northern limits of the East Sayan ice field (Gillespie *et al.* 2008; Arzhannikov *et al.* 2012; this study). This data set not only constructs a regional chronology of glacial advances around Darhad basin, but also allows detailed comparison of glacial extents

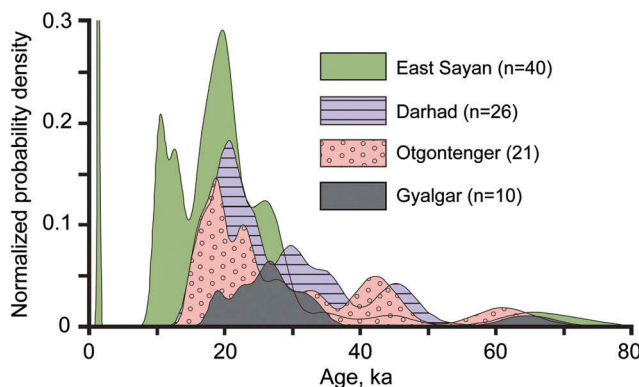


Figure 11. Summed normal distribution density of the 97^{10}Be cosmic-ray exposure ages discussed in this article. The Sayan mountain group includes the ages from Jombolok, Sailag (of 13 samples from Arzhannikov *et al.* 2012), Oka rivers, and Mönh Saridag peak. Darhad basin group includes the ages from Gillespie *et al.* (2008) and new ages from the Hoit Aguy massif and the Tengis terminal moraine. Otgontenger mountain ages are all from Rother *et al.* (2014). Gyalgar mountain ages are first reported in this article. Colour version is available online.

during various times, for example the small difference in the ELA during MIS 3 and MIS 2. These temporal and spatial patterns of glaciations in the Darhad region is similar to those in the Hangai (Rother *et al.* 2014; this study; summarized in Figure 11) suggesting that climate variations and the response of glaciers to them over all of north-central Mongolia have been similar, or smoothly varying. Palynological analysis of ^{14}C -dated lake sediments from Kotokel lake, east of Lake Baikal (Bezrukova *et al.* 2010), suggests that a cold and harsh climate dominated much of MIS 3, between \sim 45 and 35 ka, followed by drier conditions during MIS 2, at \sim 30–17 ka. This climate pattern of cold intervals both in MIS 3 and 2 is consistent with the glacial records from the Darhad and Hangai regions.

The two ^{10}Be ages for the eroded end moraine in the Sarig valley overlap within 2σ error and are direct evidence that the Tengis glacier crossed the Maly Yenisei during the LGM_G. On the east of the Maly Yenisei Gillespie *et al.* (2008) dated two boulders sitting on a wind gap at 1638 m asl to \sim 22 ka, supporting the two ^{10}Be ages from the Tengis end moraine. However, the two ^{10}Be ages from the wind gap barely overlap with each other within 2σ error, and the CRE dating of moraine boulders around Darhad basin (Gillespie *et al.* 2008) showed that there is a considerable variability of CRE ages from boulder to boulder. The high variability of CRE ages for moraine boulders around Darhad basin may suggest that the MIS 2 glaciers were stable for a long time that the boulders were deposited at different times over the span of a few thousand years.

There are beach sands at 1711 m asl on the basin wall 2.7 km south of the left-lateral Jarai moraines (Gillespie *et al.* 2008) suggesting a 175 m deep lake.

This lake would have overtopped both of the Jarai piedmont moraines, for which there is no direct evidence (Gillespie *et al.* 2008). However, a lakeshore was eroded into the younger moraine at 1679 m. Therefore, it appears that the 1711 m beach dated from early in MIS 2 and the MIS 2 lake had begun to lower by \sim 18 ka, or that 1679 m asl was the maximum MIS 2 highstand and the 1711 m highstand dated from MIS 3 or earlier. The luminescence-dated beach sands at \sim 1670 m asl near the Arsain river suggests that the lake was at least 145 m deep at \sim 14 ka. This was likely the same highstand that left the 1679 m shoreline on the Jarai moraine, and together these sites and shorelines suggest the MIS 2 lake was high, perhaps episodically, from 18 to 14 ka. It is unlikely that a continuous deep lake preceded the first Jarai moraine, since it would then likely have terminated in a calving front, and the presence of the moraine suggests that it did not.

Because the piedmont moraines at Jarai river and the Tengis end moraine at Sarig valley all date from the LGM_G, but the lake core and Shargyn cutbank evidence show older lake sediments from MIS 3, the question as to the presence of a MIS 3 moraine arises. At Hoit Aguy, the dated MIS 3 glacier was bigger than the putative MIS 2 glacier, and this suggests that the Jarai and Tengis glaciers then must have left moraine complexes roughly as large as the one from MIS 2, but if so they have not been found, and we did not see any evidence of other moraines on 15 m ASTER images. If the MIS 3 moraines were deposited close to the position of the future MIS 2 end moraines, they could have been buried. Alternatively, the MIS 3 end moraine in Sarig valley could have been placed further up valley, beyond where we travelled, or the MIS 3 glacier may have extended farther down the Maly Yenisei, its moraines having been eroded in subsequent outburst floods. However, the luminescence ages for the lake sediments in the DBC1 core do confirm the presence of a lake in Darhad during both MIS 3 and MIS 2.

Darhad basin is located at the western end of the Baikal rift, and on the eastern side of the basin an active normal fault offsets the 23.7 ± 1.5 ka Jarai moraine by 7–7.7 m (Bacon *et al.* 2003), which equates to an average slip rate of 0.31 ± 0.02 m ka^{-1} . The lake sediments at 76.9 m depth in the DBC1 core was dated to 139.6 ± 15.8 ka, a sedimentation rate of at least 0.56 ± 0.05 m ka^{-1} , not accounting for compression and erosion of the lake sediments. The subsidence of the basin floor should be more than the sedimentation in order to accommodate >200 m thick sediments. We propose that the subsidence of Darhad basin is not uniform, and the inconsistent

subsidence and uplift rates are due to 'hinging' of the basin on its western margin, where surficial evidence of faulting is less pronounced than on the east side. This mechanism requires that the Ulaan Taiga in the west must be subsiding slower than the Bayan Zürhiin ranges in the east (see details in online supplementary material: Figure S4).

There is a unique ~1 m thick layer in the DBC1 core at ~79 m depth. The layer consists of finely laminated biogenic carbonates with abundant bivalve clam fossils. The layer is almost devoid of clastic material, which suggests that the thick calcareous layer must have been biochemically precipitated in quiet and relatively warm water. The high concentration of the mollusc shells suggests that the lake was shallow at that time. It is a distinct change of depositional environment from a deep cold lake to a shallow warm lake. The lake silts below the calcareous layer, at 80.1 m depth, was dated to 135.0 ± 8.4 ka. We propose two explanations for the formation of this shallow lake: (1) it was an isolated small lake, similar to the ones found today; (2) it was a basin-wide shallow lake in a tectonically closed basin. The first hypothesis doesn't require any subsidence. However, if the second hypothesis was correct the floor of the basin-wide shallow lake must have been subsiding faster than the sedimentation of the calcareous layer. Another long core from the margins of the basin should reveal whether it was a basin-wide lake or an isolated lake. According to the second hypothesis, a subsidence rate can be estimated from the absolute elevation of the calcareous layer at ~1468 m asl (79 m below the modern ground elevation 1547 m asl). Accounting for the GPS measurement error, the calcareous layer now sits $\sim 32 \pm 5$ m below the modern sill at ~1500 m asl. In other words, the ground must have subsided 32 m or more since ~135 ka to accommodate the deposition of lake sediments. We estimate the subsidence rate in the centre of Darhad basin as $\sim 0.24 \pm 0.05$ m ka^{-1} for 10^5 -year scale, a consistent value with the 'hinged' subsidence model, considering the faster uplift rate in the east of the basin at 0.31 ± 0.02 m ka^{-1} for 10^3 -year scale.

5. Conclusions

The East Sayan mountains were glaciated extensively during MIS 2 (19–21 ka), the LGM_G, and outlet glaciers descended through the Tengis river valley and blocked the Maly Yenisei river. Ages for the end moraine in the Sarig valley and lake sediments from Darhad basin floor constrain the timing of the impounding and existence of a deep lake. The beach sands near the Arsain and

Jarai rivers constrain the depth of MIS 2 lake to at least 145 m deeper than the spillway of the modern Maly Yenisei river at 1535 m asl (Figure 12). This resolves the controversy identified by Krivonogov *et al.* (2005, 2012), which is the main factor behind this article.

The mountains around Darhad basin were also heavily glaciated during MIS 3 (~35–57 ka) and blocked the Maly Yenisei then. At Hoit Aguy, the ELA difference between the dated MIS 3 and nearby MIS 2 (?) moraine

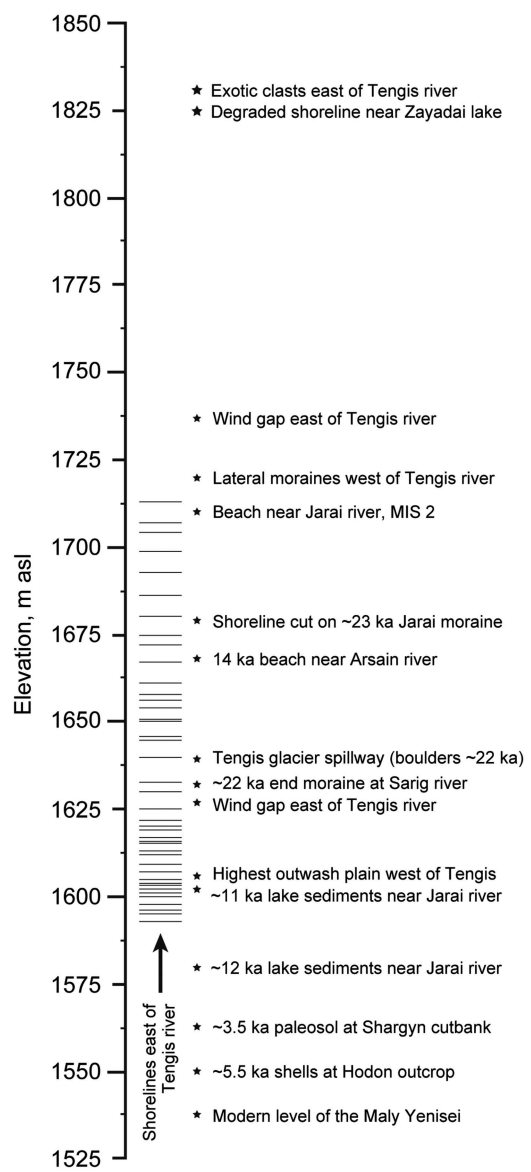


Figure 12. Shorelines and highstands of Darhad palaeolakes. Elevation of shorelines east of the Tengis river was measured by Krivonogov *et al.* (2005). The shells at Hodon outcrop was analysed by Krivonogov *et al.* (2012), and we calibrated the radiocarbon ages for comparison with the other ages. The ages from Jarai, Tengis, Shargyn rivers are from Gillespie *et al.* (2008).

was only ~50 m (2290–2240 m asl). It remains possible that the 1710 m palaeolake highstand predated the MIS 2 Jarai moraines, in which case it probably dates from MIS 3. Many unconformities and disturbances in the lake sediment record suggest the depth of the Darhad palaeolakes fluctuated frequently. The lake drained significantly after ~14 ka, and by ~4 ka Darhad basin was largely dry.

Comparison of palaeo ELAs for glaciers in central Mongolia, East Sayan mountains, and Altai mountains shows that the pattern of strong latitudinal variation of glacier extents persisted both during MIS 3 and MIS 2. Glaciers in central and northern Mongolia appear to have been more sensitive to changes in temperature than in precipitation.

Note

1. Lisiecki and Raymo (2005) defined MIS 2 as 29–14 ka, and MIS 3 as 57–29 ka. We used the term 'MIS' in its stratigraphic sense in this article.

Acknowledgements

We are grateful to the following persons for discussions and assistance with this research: Anastasia Arzhannikova (Siberian Branch, Russian Academy of Sciences), Sergei Arzhannikov (Siberian Branch, Russian Academy of Sciences), A. Bayasgalan (Mongolian University of Science and Technology), Beejinkhuu and his drilling crew (Ulaanbaatar), Raymond (Bud) Burke (Humboldt State University), James Feathers (University of Washington), Andrei Fedotov (Siberian Branch, Russian Academy of Sciences), David Fink (Australian Nuclear Science and Technology Organisation), Carrie Garrison-Laney (University of Washington), Goro Komatsu (Università d'Annunzio, Pescara, Italy), Sergey Krivonogov (Siberian Branch, Russian Academy of Sciences), Ari Matmon (The Hebrew University of Jerusalem), B. Charlotte Schreiber (University of Washington), Vladimir Sheinkman (Siberian Branch, Russian Academy of Sciences), Brian Sherrod (U.S. Geological Survey), and John Stone (University of Washington). We are especially grateful to D. Sukhbaatar and the Damdin Da Fund for the Development of Intellectual Potential (Ulaanbaatar) for continuing logistical support. We thank Victor Baker and Sergei Arzhannikov for insightful and helpful formal reviews.

Disclosure statement

No potential conflict of interest was reported by the authors.

Funding

Funding for drilling was provided by the Royalty Research Fund of the University of Washington and for CRE analysis

by a grant from the Quaternary Research Center (JW). Aspects of the research were also supported by the Terra/ASTER program operated by the Jet Propulsion Laboratory of NASA.

ORCID

Jigjidsurengiin Batbaatar  <http://orcid.org/0000-0001-7806-8361>

References

- Andrews, J.T., 1975, *Glacial systems. An approach to glaciers and their environments*: North Scituate, MA, Duxbury Press.
- Arnold, L.J., Bailey, R.M., and Tucker, G.E., 2007, Statistical treatment of fluvial dose distributions from southern Colorado arroyo deposits: *Quaternary Geochronology*, v. 2, p. 162–167. doi:[10.1016/j.quageo.2006.05.003](https://doi.org/10.1016/j.quageo.2006.05.003)
- Arzhannikov, S.G., Braucher, R., Jolivet, M., Arzhannikova, A.V., Vassallo, R., Chauvet, A., Bourlès, D., and Chauvet, F., 2012, History of late Pleistocene glaciations in the central Sayan-Tuva Upland (southern Siberia): *Quaternary Science Reviews*, v. 49, p. 16–32. doi:[10.1016/j.quascirev.2012.06.005](https://doi.org/10.1016/j.quascirev.2012.06.005)
- Auclair, M., Lamothe, M., and Huot, S., 2003, Measurement of anomalous fading for feldspar IRSL using SAR: *Radiation Measurements*, v. 37, p. 487–492. doi:[10.1016/S1350-4487\(03\)00018-0](https://doi.org/10.1016/S1350-4487(03)00018-0)
- Bacon, S.N., Bayasgalan, A., Gillespie, A., and Raymond, B., 2003, Paleoseismic displacement from landform subjected to periglacial processes: Observations along the Jarai Gol fault near the Tamyn Am Hills, Darhad Depression, northern Mongolia: XVI INQUA Congress, Geological Society of America Abstracts with Programs, Reno, NV, p. 103.
- Balco, G., 2006, Converting Al and Be isotope ratio measurements to nuclide concentrations in quartz: Documentation for CRONUS-Earth Calculator, version 2.2: http://hess.ess.washington.edu/math/docs/al_be_v22/al_be_docs.html (accessed June 2016).
- Balco, G., Stone, J.O., Lifton, N.A., and Dunai, T.J., 2008, A complete and easily accessible means of calculating surface exposure ages or erosion rates from ^{10}Be and ^{26}Al measurements: *Quaternary Geochronology*, v. 3, p. 174–195. doi:[10.1016/j.quageo.2007.12.001](https://doi.org/10.1016/j.quageo.2007.12.001)
- Banerjee, D., Murray, A.S., Bøtter-Jensen, L., and Lang, A., 2001, Equivalent dose estimation using a single aliquot of polymineral fine grains: *Radiation Measurements*, v. 33, p. 73–93.
- Batbaatar, J., and Gillespie, A.R., 2015, Outburst floods of the Maly Yenisei. Part I – review: *International Geology Review*, p. 1–30. doi:[10.1080/00206814.2015.1114908](https://doi.org/10.1080/00206814.2015.1114908)
- Batbaatar, J., Gillespie, A.R., and Schreiber, B.C., 2012, Tectonics and environment at the western end of the Baikal rift: Paleolake sediment record from Darhad Basin, northern Mongolia: *Geological Society of America Abstracts with Programs*, v. 44, no. 3, p. 56.
- Bezrukova, E.V., Tarasov, P.E., Solovieva, N., Krivonogov, S.K., and Riedel, F., 2010, Last glacial-interglacial vegetation and environmental dynamics in southern Siberia: Chronology, forcing and feedbacks: *Palaeogeography, Palaeoclimatology, Palaeoecology*, v. 296, p. 185–198. doi:[10.1016/j.palaeo.2010.07.020](https://doi.org/10.1016/j.palaeo.2010.07.020)

- Cejudo-Figueiras, C., Morales, E.A., Wetzel, C.E., Blanco, S., Hoffmann, L., and Ector, L., 2011, Analysis of the type of *Fragilaria construens* var. *subsalina* (Bacillariophyceae) and description of two morphologically related taxa from Europe and the United States: *Phycologia*, v. 50, no. 1, p. 67–77. doi:[10.2216/09-40.1](https://doi.org/10.2216/09-40.1)
- Charlesworth, J.K., 1957, The Quaternary era: London, Edward Arnold, 2 vols, p. 591, 1700.
- Clauser, C., and Huenges, E., 1995, Thermal conductivity of rocks and minerals, in Ahrens, T.J., ed., Rock physics and phase relations: A handbook of physical constants: Washington, DC, American Geophysical Union Reference Shelf, Vol. 3, p. 105–126.
- Cortes, D.D., Martin, A.I., Yun, T.S., Francisca, F.M., Santamarina, J.C., and Ruppel, C., 2009, Thermal conductivity of hydrate-bearing sediments: *Journal of Geophysical Research*, v. 114, no. B11, p. 1–10. doi:[10.1029/2008JB006235](https://doi.org/10.1029/2008JB006235)
- Ditchburn, R.G., and Whitehead, N.E., 1994, The separation of ^{10}Be from silicates, in Hancock, G., and Wallbrink, P., eds., Third Workshop of the South Pacific Environmental Radioactivity Association: Canberra, Australian National University, p. 4–7.
- Edlund, M.B., Williams, R.M., and Soninkhishig, N., 2003, The planktonic diatom diversity of ancient Lake Hovsgol, Mongolia: *Phycologia*, v. 42, p. 232–260. doi:[10.2216/i0031-8884-42-3-232.1](https://doi.org/10.2216/i0031-8884-42-3-232.1)
- Farr, T.G., Rosen, P.A., Caro, E., Crippen, R., Duren, R., Hensley, S., Kobrick, M., Paller, M., Rodriguez, E., Roth, L., Seal, D., Shaffer, S., Shimada, J., Umland, J., Werner, M., Oskin, M., Burbank, D., and Alsdorf, D., 2007, The shuttle radar topography mission: *Reviews of Geophysics*, v. 45, no. 2, p. 1–33. doi:[10.1029/2005RG000183](https://doi.org/10.1029/2005RG000183)
- Feathers, J.K., Casson, M.A., Schmidt, A.H., and Chithambo, M.L., 2012, Application of pulsed OSL to polymimetal fine-grained samples: *Radiation Measurements*, v. 47, p. 201–209. doi:[10.1016/j.radmeas.2012.01.003](https://doi.org/10.1016/j.radmeas.2012.01.003)
- Feathers, J.K., and Pagonis, V., 2015, Dating quartz near saturation – Simulations and application at archaeological sites in South Africa and South Carolina: *Quaternary Geochronology*, v. 30, p. 416–421. doi:[10.1016/j.quageo.2014.12.008](https://doi.org/10.1016/j.quageo.2014.12.008)
- Fridleifsson, I.B., Bertani, R., Huenges, E., Lund, J.W., and Rybach, L., 2008, The possible role and contribution of geothermal energy to the mitigation of climate change, in Hohmeyer, O., and Trittin, T., eds., Proceedings of IPCC Scoping meetings on renewable energy sources, Lübeck, Germany, p. 59–80.
- Galbraith, R.F., 1988, Graphical display of estimates having differing standard errors: *Technometrics*, v. 30, p. 271–281.
- Galbraith, R.F., and Green, P.F., 1990, Estimating the component ages in a finite mixture: *International Journal of Radiation Applications and Instrumentation. Part D. Nuclear Tracks and Radiation Measurements*, v. 17, p. 197–206. doi:[10.1016/1359-0189\(90\)90035-V](https://doi.org/10.1016/1359-0189(90)90035-V)
- Galbraith, R.F., and Roberts, R.G., 2012, Statistical aspects of equivalent dose and error calculation and display in OSL dating: An overview and some recommendations: *Quaternary Geochronology*, v. 11, p. 1–27. doi:[10.1016/j.quageo.2012.04.020](https://doi.org/10.1016/j.quageo.2012.04.020)
- Gillespie, A.R., Burke, R.M., Komatsu, G., and Bayasgalan, A., 2008, Late Pleistocene glaciers in Darhad Basin, northern Mongolia: *Quaternary Research*, v. 69, p. 169–187. doi:[10.1016/j.yqres.2008.01.001](https://doi.org/10.1016/j.yqres.2008.01.001)
- Gillespie, A.R., 1991, Testing a new climatic interpretation for the Tahoe glaciation, in Hall Jr., C.A., Doyle-Jones, V., and Widawski, B., eds., Natural history of Eastern California and high-altitude research, White Mountain Research Station symposium, Volume 3: Los Angeles, CA, University of California, p. 383–398.
- Gillespie, A.R., and Molnar, P., 1995, Asynchronous maximum advances of mountain and continental glaciers: *Reviews of Geophysics*, v. 33, p. 311–364. doi:[10.1029/95RG00995](https://doi.org/10.1029/95RG00995)
- Gillespie, A.R., Rupper, S., and Roe, G., 2003, Climatic interpretation from mountain glaciations in Central Asia: *Geological Society of America Abstracts with Programs*, v. 35, p. 414.
- Gravis, G.F., and Lisun, A.M., 1974, Ritmostratigrafiya chetvertichnykh otlozheniy Mongoli po palinologicheskim dannym i istoriya razvitiya mnogoletnemeryzhlykh gornykh porod (Rhythmic-stratigraphy of Quaternary sediments in Mongolia according to palynological evidence and evolution history of permafrost), in Melnikov, P.I., ed., Geocryological conditions of Mongolian People's Republic, Transactions of the Joint Soviet-Mongolian Scientific-Research Geological Expedition, Volume 10: Moscow, Nauka, p. 148–186. (in Russian).
- Gross, G., Kerschner, H., and Patzelt, G., 1976, Methodische Untersuchungen über die Schneegrenze in alpinen Gletschergebieten: *Zeitschrift für Gletscherkunde und Glazialgeologie*, v. 12, p. 223–251.
- Grosswald, M.G., and Rudoy, A.N., 1996, Quaternary glacier-dammed lakes in the mountains of Siberia: *Polar Geography*, v. 20, p. 180–198. doi:[10.1080/10889379609377599](https://doi.org/10.1080/10889379609377599)
- Guiry, M.D., and Guiry, G.M., 2015, AlgaeBase. World-wide electronic publication: Galway, National University of Ireland: <http://www.algaebase.org> ((accessed September 2015)).
- Hallet, B., and Putkonen, J., 1994, Surface dating of dynamic landforms: Young boulders on aging moraines: *Science*, v. 265, p. 937–940. doi:[10.1126/science.265.5174.937](https://doi.org/10.1126/science.265.5174.937)
- Harris, I., Jones, P.D., Osborn, T.J., and Lister, D.H., 2014, Updated high-resolution grids of monthly climatic observations – The CRU TS3.10 dataset: *International Journal of Climatology*, v. 34, p. 623–642. doi:[10.1002/joc.3711](https://doi.org/10.1002/joc.3711)
- Heyman, J., 2014, Paleoglacieration of the Tibetan Plateau and surrounding mountains based on exposure ages and ELA depression estimates: *Quaternary Science Reviews*, v. 91, p. 30–41. doi:[10.1016/j.quascirev.2014.03.018](https://doi.org/10.1016/j.quascirev.2014.03.018)
- Hülle, D., Hilgers, A., Radtke, U., Stoltz, C., Hempelmann, N., Grunert, J., Felauer, T., and Lehmkuhl, F., 2010, OSL dating of sediments from the Gobi Desert, Southern Mongolia: *Quaternary Geochronology*, v. 5, p. 107–113. doi:[10.1016/j.quageo.2009.06.002](https://doi.org/10.1016/j.quageo.2009.06.002)
- Huntley, D.J., and Lamothe, M., 2001, Ubiquity of anomalous fading in K-feldspars and the measurement and correction for it in optical dating: *Canadian Journal of Earth Sciences*, v. 38, p. 1093–1106. doi:[10.1139/e01-013](https://doi.org/10.1139/e01-013)
- Ishikawa, M., and Yamkhin, J., 2015, Formation chronology of Arsain pingo, Darhad basin, northern Mongolia: Permafrost and Periglacial Processes. doi:[10.1002/ppp.1877](https://doi.org/10.1002/ppp.1877)
- Jacobs, Z., Duller, G.A.T., and Wintle, A.G., 2006, Interpretation of single grain D_e distributions and calculation of D_e :



- Radiation Measurements, v. 41, p. 264–277. doi:[10.1016/j.radmeas.2005.07.027](https://doi.org/10.1016/j.radmeas.2005.07.027)
- Komatsu, G., Arzhannikov, S.G., Gillespie, A.R., Burke, R.M., Miyamoto, H., and Baker, V.R., 2009, Quaternary paleolake formation and cataclysmic flooding along the upper Yenisei River: *Geomorphology*, v. 104, p. 143–164. doi:[10.1016/j.geomorph.2008.08.009](https://doi.org/10.1016/j.geomorph.2008.08.009)
- Krivenogov, S.K., Sheinkman, V.S., and Mistryukov, A.A., 2005, Ice damming of the Darhad paleolake (northern Mongolia) during the Late Pleistocene: *Quaternary International*, v. 136, p. 83–94. doi:[10.1016/j.quaint.2004.11.010](https://doi.org/10.1016/j.quaint.2004.11.010)
- Krivenogov, S.K., Yi, S., Kashiwaya, K., Kim, J.C., Narantsetseg, T., Oyunchimeg, T., Safonova, I.Y., Kazansky, A.Y., Sitnikova, T., Kim, J.Y., and Hasebe, N., 2012, Solved and unsolved problems of sedimentation, glaciation and paleolakes of the Darhad Basin, Northern Mongolia: *Quaternary Science Reviews*, v. 56, p. 142–163. doi:[10.1016/j.quascirev.2012.08.013](https://doi.org/10.1016/j.quascirev.2012.08.013)
- Lehmkuhl, F., Hilgers, A., Fries, S., Hülle, D., Schütz, F., Shumilovskikh, L., Felauer, T., and Protze, J., 2011, Holocene geomorphological processes and soil development as indicator for environmental change around Karakorum, Upper Orkhon Valley (Central Mongolia): *Catena*, v. 87, p. 31–44. doi:[10.1016/j.catena.2011.05.005](https://doi.org/10.1016/j.catena.2011.05.005)
- Lisiecki, L.E., and Raymo, M.E., 2005, A Pliocene-Pleistocene stack of 57 globally distributed benthic $\delta^{18}\text{O}$ records: *Paleoceanography*, v. 20, p. PA1003. doi:[10.1029/2004PA001071](https://doi.org/10.1029/2004PA001071)
- Lüthgens, C., Kröbtschek, M., Böse, M., and Fuchs, M.C., 2010, Optically stimulated luminescence dating of fluvioglacial (sandur) sediments from north-eastern Germany: *Quaternary Geochronology*, v. 5, p. 237–243. doi:[10.1016/j.quageo.2009.06.007](https://doi.org/10.1016/j.quageo.2009.06.007)
- Manley, G., 1959, The late-glacial climate of north-west England: *Liverpool and Manchester Geological Journal*, v. 2, p. 188–215. doi:[10.1002/gj.3350020207](https://doi.org/10.1002/gj.3350020207)
- Meier, M.F., and Post, A.S., 1962, Recent variations in mass net budgets of glaciers in western North America: *International Association of Hydrological Sciences Publication*, v. 58, p. 63–77.
- Meierding, T.C., 1982, Late pleistocene glacial equilibrium-line altitudes in the Colorado Front Range: A comparison of methods: *Quaternary Research*, v. 18, p. 289–310. doi:[10.1016/0033-5894\(82\)90076-X](https://doi.org/10.1016/0033-5894(82)90076-X)
- Merle, J.R., 2001, Quaternary geology of the Tengis-Shishid Gol region, Khovsgol, Mongolia [Thesis B.A.]: Walla Walla, WA, Whitman College, p. 56.
- National Aeronautics and Space Administration, 2015, The ASTER L1B data product was retrieved from the online Data Pool, courtesy of the NASA Land Processes Distributed Active Archive Center (LP DAAC), USGS/Earth Resources Observation and Science (EROS) Center, Sioux Falls, South Dakota: https://lpdaac.usgs.gov/data_access/data_pool (accessed June 2016). ASTER GDEM is a product of METI, Japan and NASA, USA.
- O'Connor, J.E., and Costa, J.E., 2004, The world's largest floods – Their causes and magnitudes: U.S. Geological Survey Circular 1254: Reston, VA, U.S. Geological Survey, p. 13.
- Peck, J.A., King, J.W., Colman, S.M., and Kravchinsky, V.A., 1994, A rock-magnetic record from Lake Baikal, Siberia: Evidence for Late Quaternary climate change: *Earth and Planetary Science Letters*, v. 122, p. 221–238. doi:[10.1016/0012-821X\(94\)90062-0](https://doi.org/10.1016/0012-821X(94)90062-0)
- Peretolchin, S.P., 1908, Ledniki hrepta Munku-Sardyk (Glaciers of the Munku-Sardyk ridge): Tomsk, Izvestiya Tomskogo Teknologicheskogo Instituta (Proceedings of the Tomsk Technological Institute), v. 9, no. 1, p. 47. (in Russian).
- Porter, S.C., 1975, Equilibrium line altitudes of late Quaternary glaciers in the Southern Alps, New Zealand: *Quaternary Research*, v. 5, p. 27–47. doi:[10.1016/0033-5894\(75\)90047-2](https://doi.org/10.1016/0033-5894(75)90047-2)
- Porter, S.C., 2001, Snowline depression in the tropics during the Last Glaciation: *Quaternary Research*, v. 20, p. 1067–1091.
- Prokopenko, A.A., Karabanov, E.B., Kuz'min, M.I., and Williams, D.F., 2001, The mechanism of early glaciation during the transition from Kazantsevo climatic optimum to Zyrjanka glacial period (Evidence from bottom sediments of Lake Baikal): *Geologiya i Geofizika* (Russian Geology and Geophysics), v. 42, no. 1–2, p. 64–75 (55–65).
- Putkonen, J., and Swanson, T., 2003, Accuracy of cosmogenic ages for moraines: *Quaternary Research*, v. 59, p. 255–261. doi:[10.1016/S0033-5894\(03\)00006-1](https://doi.org/10.1016/S0033-5894(03)00006-1)
- Ramage, J.M., Smith, J.A., Rodbell, D.T., and Seltzer, G.O., 2005, Comparing reconstructed Pleistocene equilibrium-line altitudes in the tropical Andes of central Peru: *Journal of Quaternary Science*, v. 20, p. 777–788. doi:[10.1002/\(ISSN\)1099-1417](https://doi.org/10.1002/(ISSN)1099-1417)
- Reimer, P.J., Bard, E., Bayliss, A., Beck, J.W., Blackwell, P.G., Ramsey, C.B., Buck, C.E., Cheng, H., Edwards, R.L., Friedrich, M., Grootes, P.M., Guilderson, T.P., Haflidason, H., Hajdas, I., Hatté, C., Heaton, T.J., Hoffmann, D.L., Hogg, A.G., Hughen, K.A., Kaiser, K.F., Kromer, B., Manning, S.W., Niu, M., Reimer, R.W., Richards, D.A., Scott, E.M., Southon, J.R., Staff, R.A., Turney, C.S.M., and Plicht, J., 2013, IntCal13 and MARINE13 radiocarbon age calibration curves 0–50,000 years cal BP: *Radiocarbon*, v. 55, no. 4, p. 1869–1887. doi:[10.2458/azu_js_rc.55.16947](https://doi.org/10.2458/azu_js_rc.55.16947)
- Rother, H., Lehmkuhl, F., Fink, D., and Nottebaum, V., 2014, Surface exposure dating reveals MIS-3 glacial maximum in the Khangai Mountains of Mongolia: *Quaternary Research*, v. 82, p. 297–308. doi:[10.1016/j.yqres.2014.04.006](https://doi.org/10.1016/j.yqres.2014.04.006)
- Round, F.E., and Bukhtiyarova, L., 1996, Four new genera based on Achnanthes (Achnanthidium) together with a redefinition of Achnanthidium: *Diatom Research*, v. 11, p. 345–361. doi:[10.1080/0269249X.1996.9705389](https://doi.org/10.1080/0269249X.1996.9705389)
- Rupper, S., and Koppes, M., 2010, Spatial patterns in Central Asian climate and equilibrium line altitudes: *IOP Conference Series: Earth and Environmental Science*, v. 9, no. 012009. doi:[10.1088/1755-1315/9/1/012009](https://doi.org/10.1088/1755-1315/9/1/012009)
- Rupper, S., and Roe, G., 2008, Glacier changes and regional climate: A mass and energy balance approach: *Journal of Climate*, v. 21, p. 5384–5401. doi:[10.1175/2008JCLI2219.1](https://doi.org/10.1175/2008JCLI2219.1)
- Rupper, S., Roe, G., and Gillespie, A., 2009, Spatial patterns of Holocene glacier advance and retreat in Central Asia: *Quaternary Research*, v. 72, p. 337–346. doi:[10.1016/j.yqres.2009.03.007](https://doi.org/10.1016/j.yqres.2009.03.007)
- Sakai, A., Nuimura, T., Fujita, K., Takenaka, S., Nagai, H., and Lamsal, D., 2015, Climate regime of Asian glaciers revealed by GAMDAM glacier inventory: *The Cryosphere*, v. 9, p. 865–880. doi:[10.5194/tc-9-865-2015](https://doi.org/10.5194/tc-9-865-2015)
- Sharkhuu, A., Sharkhuu, N., Etzelmüller, B., Heggem, E.S.F., Nelson, F.E., Shiklomanov, N.I., Goulden, C.E., and Brown, J., 2007, Permafrost monitoring in the Hovsgol mountain

- region, Mongolia: *Journal of Geophysical Research*, v. 112, p. F02S06. doi:[10.1029/2006JF000543](https://doi.org/10.1029/2006JF000543)
- Shchetnikov, A.A., 2001, Struktura reliefs i noveyshaya tektonika Tunkinskogo rifta (Structure of relief and neotectonics of the Tunka Rift) [Abstract of PhD thesis]: Irkutsk, Institute of Earth's Crust, Siberian Branch, Russian Academy of Sciences, p. 19. (in Russian).
- Stone, J., 2000, Air pressure and cosmogenic isotope production: *Journal of Geophysical Research: Solid Earth*, v. 105, no. B10, p. 23753–23759. doi:[10.1029/2000JB900181](https://doi.org/10.1029/2000JB900181)
- Stuiver, M., and Polach, H.A., 1977, Discussion: Reporting of ^{14}C data: *Radiocarbon*, v. 19, p. 355.
- Stuiver, M., and Reimer, P.J., 1993, Extended ^{14}C database and revised CALIB radiocarbon calibration program: *Radiocarbon*, v. 35, p. 215–230.
- Thomas, P.J., Murray, A.S., and Sandgren, P., 2003, Age limit and age underestimation using different OSL signals from lacustrine quartz and polymineral fine grains: *Quaternary Science Reviews*, v. 22, p. 1139–1143. doi:[10.1016/S0277-3791\(03\)00045-3](https://doi.org/10.1016/S0277-3791(03)00045-3)
- Torsnes, I., Rye, N., and Nesje, A., 1993, Modern and Little Ice Age equilibrium-line altitudes on outlet valley glaciers from Jostedalsbreen, western Norway: An evaluation of different approaches to their calculation: *Arctic and Alpine Research*, v. 25, p. 106–116. doi:[10.2307/1551546](https://doi.org/10.2307/1551546)
- Ufland, A.K., Ilyin, A.V., and Spirkin, A.I., 1969, Vpadiny baikal'skogo tipa severnoi Mongolii (Baikal-type basins of northern Mongolia): *Bulletin of the Moscow Society of Naturalists (MOIP)*, Geology series, Moscow, Moscow University Publ., v. 44, no. 6, p. 5–22. (in Russian).
- Ufland, A.K., Ilyin, A.V., Spirkin, A.I., and Shilova, G.N., 1971, Osnovniye cherty stratigrafii i usloviya formirovanya Kainozoiskikh obrazovanii Prikozogolya (MNR) (Main features of stratigraphy and formation of Cenozoic deposits in Prekosogol) (MPR): *Bulletin of the Moscow Society of Naturalists (MOIP)*, Geology Series, Moscow, Moscow University Publ., v. 46, p. 54–69. (in Russian).
- Vasil'chuk, Y.K., Alekseev, S.V., Arzhannikov, S.G., Alekseeva, L.P., Budantseva, N.A., Chizhova, J.N., Arzhannikova, A.V., Vasil'chuk, A.C., Kozyreva, E.A., Rybchenko, A.A., and Svetlakov, A.A., 2015, Oxygen and hydrogen isotope compositions of lithals frozen core: A case study from the Sentsa River valley, East Sayan: *Kriosfera Zemli (Earth's Cryosphere)*, v. 19, no. 2, p. 46–58.
- Verosub, K.L., and Roberts, A.P., 1995, Environmental magnetism: Past, present, and future: *Journal of Geophysical Research: Solid Earth*, v. 100, no. B2, p. 2175–2192. doi:[10.1029/94JB02713](https://doi.org/10.1029/94JB02713)
- Wallinga, J., Murray, A.S., Duller, G.A.T., and Törnqvist, T.E., 2001, Testing optically stimulated luminescence dating of sand-sized quartz and feldspar from fluvial deposits: *Earth and Planetary Science Letters*, v. 193, p. 617–630. doi:[10.1016/S0012-821X\(01\)00526-X](https://doi.org/10.1016/S0012-821X(01)00526-X)
- Wegmann, K.W., Amgaa, T.S., Frankel, K.L., Dewett, A.P., and Bayasgalan, A., 2011, Geologic, geomorphic, and environmental change at the northern termination of the Lake Hövsgöl rift, Mongolia, in *Proceedings of the Twenty-Fourth Annual Keck Research Symposium in Geology*, Union College, Schenectady, NY, April, 2011, p. 220–229.
- Wintle, A.G., and Murray, A.S., 2006, A review of quartz optically stimulated luminescence characteristics and their relevance in single- aliquot regeneration dating protocols: *Radiation Measurements*, v. 41, p. 369–391. doi:[10.1016/j.radmeas.2005.11.001](https://doi.org/10.1016/j.radmeas.2005.11.001)

Appendix

Table A1. ^{10}Be data.

Sample identification	Latitude N / Longitude E (decimal degrees)	Altitude (m asl)	Lithology	Sample thickness (cm)	Shielding correction factor	Quartz (g)	Be carrier (mg)	$^{10}\text{Be}/^{9}\text{Be} \times 10^{-15}$	standard	$[^{10}\text{Be}] \pm 1\sigma (10^3 \text{ atoms g}^{-1})$
070402-ag-RMS-1	51.736086 / 100.599854	2640	Granodiorite	2.5	0.99	30.009	0.2960	629.10 ± 28.00	NIST_27900	414.6 ± 20.7
070402-ag-RMS-2	51.736086 / 100.599854	2640	Granodiorite	2.5	0.99	30.003	0.2950	629.90 ± 14.20	NIST_27900	413.9 ± 13.1
070402-ag-RMS-3	51.730918 / 100.600332	2800	Granodiorite	2.5	0.99	30.071	0.2950	611.50 ± 18.60	NIST_27900	400.9 ± 15.1
070402-ag-RMS-4	51.730918 / 100.600332	2800	Granodiorite	2.5	0.99	22.481	0.2950	444.70 ± 21.70	NIST_27900	389.9 ± 20.9
070402-ag-RMS-5	51.730918 / 100.600332	2800	Granodiorite	2.5	0.99	13.931	0.2940	258.40 ± 11.60	NIST_27900	364.4 ± 18.3
070402-ag-RMS-6	51.728600 / 100.598324	2900	Granodiorite	2.5	0.99	22.533	0.2950	67.50 ± 5.50	NIST_27900	59.1 ± 5.0
070402-ag-RMS-7	51.728600 / 100.598324	2900	Quartz vein	2.5	0.99	20.013	0.2902	51.03 ± 3.54	NIST_27900	49.4 ± 3.6
070402-ag-RMS-8A	51.738667 / 100.600355	2640	Quartz vein	2.5	0.99	30.065	0.2930	1355.20 ± 26.30	NIST_27900	882.5 ± 26.1
070402-ag-RMS-8B	51.738667 / 100.600355	2640	Quartz vein	2.5	0.99	20.008	0.2911	693.32 ± 13.71	NIST_27900	674.1 ± 20.1
070402-ag-RMS-9	51.738667 / 100.600355	2640	Quartz vein	2.5	0.99	18.781	0.2890	925.50 ± 13.30	NIST_27900	951.6 ± 25.3
070802-ag-RSLIK-1	52.788700 / 99.736472	1454	Granite	1.0	0.99	16.410	0.2310	316.00 ± 11.30	NIST_27900	297.2 ± 12.5
070802-ag-RSLIK-2	52.788700 / 99.736472	1454	Red granite	2.5	0.99	15.597	0.2330	320.00 ± 11.80	NIST_27900	319.4 ± 13.8
070802-ag-RSLIK-3	52.788700 / 99.736472	1464	Red granite	7.5	1.00	19.559	0.2320	357.50 ± 12.30	NIST_27900	283.4 ± 11.6
070802-ag-RSLIK-4	52.788700 / 99.736472	1454	Red granite	2.0	1.00	14.580	0.2310	857.20 ± 22.80	NIST_27900	907.5 ± 31.5
070802-ag-RSLIK-5	52.788700 / 99.736472	1454	Red granite	10	1.00	18.654	0.2330	319.60 ± 11.60	NIST_27900	266.8 ± 11.4
070802-ag-RSLIK-6	52.784657 / 99.732189	1454	Red granite	5.0	1.00	14.937	0.2310	190.30 ± 7.30	NIST_27900	196.7 ± 8.7
070802-ag-RSLIK-7	52.784657 / 99.732189	1454	Red granite	5.0	1.00	22.119	0.2290	331.10 ± 9.80	NIST_27900	229.1 ± 8.5
070802-ag-RSLIK-8	52.784657 / 99.732189	1454	Diorite	2.5	1.00	10.004	0.1470	180.00 ± 15.70	NIST_27900	176.7 ± 15.9
070802-ag-RSLIK-10	52.784657 / 99.732189	1454	Granodiorite	2.5	1.00	18.479	0.2340	314.30 ± 12.00	NIST_27900	266.0 ± 11.8
071002-ag-RDIO-1	52.731073 / 99.615047	1410	Granodiorite	1.0	1.00	25.084	0.2890	356.60 ± 14.00	NIST_27900	274.5 ± 12.4
071002-ag-RDIO-2	52.731073 / 99.615047	1410	Granodiorite	1.0	1.00	25.092	0.2950	366.20 ± 14.10	NIST_27900	287.7 ± 12.8
071002-ag-RDIO-3	52.731073 / 99.615047	1410	Granite	3.0	1.00	25.044	0.2930	599.00 ± 36.40	NIST_27900	468.3 ± 30.3
071002-ag-RDIO-5	52.731073 / 99.615047	1410	Granodiorite	1.0	1.00	6.176	0.1460	201.40 ± 13.50	NIST_27900	318.1 ± 22.5
071002-ag-RDIO-6	52.71717833 / 99.599533	1392	Granodiorite	8.0	1.00	12.667	0.2330	204.60 ± 6.60	NIST_27900	253.6 ± 10.0
071202-ag-ROKA-06	52.298633 / 100.224617	1518	Gneiss	5.0	0.99	20.880	0.2873	258.80 ± 11.14	NIST_27900	238.0 ± 11.5
080709-HA-JB-02	51.552057 / 98.714686	2332	Granite	2.5	1.00	17.572	0.2135	1206.80 ± 23.40	07KNSTD	979.9 ± 29.0
080709-HA-JB-03	51.552057 / 98.714686	2335	Granite	2.5	1.00	5.924	0.2121	387.31 ± 16.54	07KNSTD	926.6 ± 44.7
150707-DB-ag-003A	51.453579 / 99.038698	1631	Granite	5.0	0.99	10.630	0.2509	237.10 ± 3.89	07KNSTD	374.0 ± 10.4
150707-DB-ag-003C	51.453579 / 99.038698	1631	Granite	5.0	0.99	10.166	0.2511	196.40 ± 5.15	07KNSTD	324.2 ± 11.2
6-25-02-ag-JG01a	51.595383 / 99.986200	2459	Granitic	1.0	1.00	10.619	0.2544	820.7 ± 124.8	07KNSTD	1313.7 ± 283.1
6-25-02-ag-JG01b	51.595383 / 99.986200	2459	Granitic	2.5	1.00	11.843	0.2724	354.2 ± 10.0	07KNSTD	544.5 ± 23.1
ZAG-ARG-01c	51.595383 / 99.986200	2459	Quartz vein	1.0	1.00	11.129	0.2385	290.9 ± 9.7	07KNSTD	451.6 ± 22.2
ZAG-ARG-01A	48.183767 / 98.781450	2472	Granite	4.0	0.99	14.075	0.2419	643.09 ± 16.12	KNSTD	756.9 ± 28.9
ZAG-ARG-01B	48.183767 / 98.781450	2472	Granite	4.0	0.99	14.962	0.2502	562.76 ± 10.65	KNSTD	628.7 ± 19.0
ZAG-ARG-02B	48.120000 / 98.813347	2285	Granite	4.0	0.99	13.272	0.2495	375.38 ± 9.82	KNSTD	471.5 ± 18.7
ZAG-ARG-03A	48.118050 / 98.815833	2253	Pink granite	4.0	0.99	12.835	0.2507	462.511 ± 8.49	KNSTD	603.6 ± 35.2
ZAG-ARG-03B	48.118050 / 98.815833	2253	Granite	4.0	0.99	14.361	0.2501	351.360 ± 98.96	KNSTD	408.82 ± 172.8
ZAG-ARG-04B	48.129017 / 98.798217	2332	Granite	4.0	0.99	14.293	0.2500	674.44 ± 15.70	KNSTD	788.3 ± 28.2
ZAG-SB-04A	48.182884 / 98.804676	2585	Granite	4.0	0.99	13.275	0.2506	680.47 ± 11.80	KNSTD	858.4 ± 24.3
ZAG-SB-04B	48.182884 / 98.804676	2585	Granite	4.0	0.99	14.583	0.2507	144.15 ± 17.11	KNSTD	1660.1 ± 36.4
ZAG-SB-04C	48.182884 / 98.804676	2585	Granite	4.0	0.99	15.082	0.2502	632.23 ± 10.98	KNSTD	700.7 ± 19.9
ZAG-SB-05	48.195113 / 98.792166	2815	Granite	4.0	0.99	14.810	0.2504	3872.7 ± 145.43	KNSTD	4374.8 ± 95.4

We used 2.7 g cm⁻³ for sample density. Using 2.6 g cm⁻³ would make less than 0.3% difference in the apparent age for samples <10 cm thick.

Table A2. Sedimentation breaks in the DBC1 core.
The scale is in cm.

Depth, m	Type of sedimentation break	Photograph
9.1	Slumping	
27.5	Tilted bed	
27.7	Tilted bed	
30.4	Cross bedding	
31.0	Cross bedding	
32.3	Large clast (drop stone?)	
35.1	Slumping	
35.3	Slumping	
35.6	Slumping	
36.7	Slumping	
38.1	Slumping	
41.6	Cross bedding	
43.6	Abrupt end of lamination	

(Continued)

Table A2. (Continued).

Depth, m	Type of sedimentation break	Photograph
45.7	Turbidity flow	
46.9	Erosion	
50.0	Slumping (deformation)	
50.1	Erosion	
70.9	Erosion	
71.3	Cross bedding	
76.7	Cross bedding	
80.6	Deformation	
81.7	Micro fault	
81.8	Erosion	

Table A3. Luminescence ages ($ka \pm 2\sigma$) for the Darhad basin samples, estimated from single-grain coarse quartz and feldspar, and from multi-mineral aliquots. Ages estimated using a finite mixture model (Galbraith 1988; Jacobs *et al.* 2006) are given with the component and its percentage in parentheses. Ages from the coarse feldspar and multi-mineral aliquots are all corrected for anomalous fading (Huntley and Lamothe 2001). Reasoning for the assigned deposition ages is discussed in detail in Section 3.2.

Sample identification ^a	Coarse single-grain SAR ages (ka)			Fine multi-mineral aliquot ages (ka)			Assigned deposition age (ka, as in Table 1)
	Quartz	n	Feldspar	n	OSL	IRSL	
DBC1B 9.15 (UW1264) (deep-water lake sediment)	18.3 ± 4.0 (central)	2	19.5 ± 2.6 (minimum) 46.2 ± 2.0 (2nd: 94%)	83	28.0 ± 2.1	48.9 ± 5.9	19.5 ± 2.6
DBC1B 9.50 (UW1867) (deep-water lake sediment)	28.2 ± 4.0 (central)	5	30.9 ± 3.1 (minimum) 46.5 ± 1.9 (2nd: 93%)	114	–	–	30.9 ± 3.1
DBC1A 43.7 (UW1265) (deep-water lake sediment)	34.7 ± 8.1 (minimum) 100.9 ± 18.3 (central) 34.5 ± 6.8 (1st: 18.4%) 104.7 ± 11.5 (2nd: 66%)	21	70.3 ± 16.0 (1st: 100%)	5	–	–	34.7 ± 8.1
DBC1A 46.8 (UW1292) (deep-water lake sediment)	45.2 ± 10.1 (minimum) 103.6 ± 24.4 (central) 79.7 ± 9.5 (1st: 83%)	13	45.2 ± 9.7 (minimum) 101.6 ± 8.2 (1st: 100%)	59	–	–	45.2 ± 9.7
DBC1A 76.9 (UW1293) (shallow (?) lake sediment)	–	–	–	–	126.5 ± 19.8	162.8 ± 26.4	139.6 ± 15.8 (weighted average)
DBC1A 80.1 (UW2702) (deep-water lake sediment)	–	–	–	–	56.5 ± 4.2	135.0 ± 8.4	135.0 ± 8.4
DB-AG-2004-03A (UW1868) (beach sand)	14.7 ± 4.5 (central)	2	14.3 ± 1.7 (minimum) 16.0 ± 1.1 (1st: 100%)	138	–	–	14.3 ± 1.7
DB-AG-2007-002 (UW1872) (moraine till)	11.9 ± 7.5 (minimum) 57.5 ± 27.2 (central) 8.3 ± 4.5 (1st: 20%) 81.7 ± 21.0 (2nd: 52%)	6	12.0 ± 7.5 (minimum) 72.8 ± 3.5 (1st: 100%)	25	–	–	12.0 ± 7.5 (age is minimum)

^aUniversity of Washington laboratory numbers and the depositional environments are given in the parentheses.